International Journal of Earth Sciences (2023) 112:345–382
https://doi.org/10.1007/s00531-022-02253-7

ORIGINAL PAPER

Timing of rapid cooling and erosional decay of two volcanic islands of the Canary Archipelago: implications from low-temperature thermochronology

Sherif Mansour[1,2] · Ulrich A. Glasmacher[1] · Florian C. Krob[1] · Ramón Casillas[3] · Marie Albinger[1]

Received: 25 August 2021 / Accepted: 4 October 2022 / Published online: 27 October 2022

Abstract

The Canary Archipelago comprises seven volcanic islands formed by the activity of the Canary mantle anomaly that might have been caused by an ascending plume at the NW-African passive margin. The "Basal Complex (BC)", which contains the islands pre-shield rock formations, is exposed in the northwest and central Fuerteventura and NW-La Gomera and preserves the archive of giant landslides that caused the removal of most of the shield-stage volcanic rocks. Tools, like low-temperature thermochronology (LTT) are sensitive to rapid cooling activities that accompany landslides. In addition, integrating LTT data with time–temperature (*t–T*) numerical modelling are a powerful tool for reconstructing the thermo-tectonic evolution as well as defining and quantifying long-term landscape evolution in a variety of geological settings. To unravel part of the long-term landscape evolution of Fuerteventura and La Gomera, zircon and apatite fission-track, and (U–Th)/He data combined with *t–T* numerical modelling were applied to 39 samples representing the main rock units of the BCs and younger magmatic rocks on both islands. In Fuerteventura, the Northwest and Central Basal Complexes reveal rapid cooling/exhumation of more than 200 °C at ~ 20 Ma. The quantification of the thickness of the rock column using the *t–T* cooling path would need the knowledge of the palaeo-heat flow. The published thickness of the moved rock column in Fuerteventura and La Gomera does not point to an extreme high heat flow. Therefore, the formation of a giant landslide leads to the removal of ~ 2.0 (± 0.5) km of the volcano rock column. Offshore, such a landslide has led to part of the Puerto Rosario large debris avalanche. The "Central Basal Complex" revealed two more rapid cooling/exhumation events at ~ 16 Ma and ~ 14 Ma that might also be related to landslides. The three landslides might be responsible for the formation of the nowadays Puerto Rosario Debris Avalanche Unit offshore. What might have caused the landslides in Fuerteventura. Age data published provide evidence for magmatic and tectonic activity that occur at the time of the formation of the giant landslides. In addition, the Miocene climate significant changes lead to changes in precipitation, and such changes might also provide a destabilisation of pyroclastic units. Therefore, the causes of the giant landslides might be related to more than only one process. The La Gomera BC has experienced two rapid cooling/exhumation events: the first at ~ 9 Ma, which might have caused ~ 2.0 (± 0.2) km of erosion forming the offshore Tazo avalanche, also known as the Tazo landslide. The second rapid cooling at ~ 8.0 Ma is located at the northwest of the Island and might have been caused by the Garajonay caldera collapse and followed by landslides. The landslides are assumed to have formed the Segments I, II, III, and VIII of the submarine debris avalanches offshore. Like Fuerteventura, both landslides might have been triggered by tectonic and magmatic activities as well as due to variation in precipitation caused by climate variation.

Keywords Low-temperature thermochronology · Fuerteventura · La Gomera · Volcanic island decay · Giant landslides · Time–temperature evolution

Introduction

Giant landslides often cause the denudation of volcanic edifice on volcanic islands by rapid erosion (Moore 1964; Lipman et al. 1988; Inokuchi 1988; Moore et al. 1989, 1994; Iverson 1991, 1995; McGuire 1996; Krastel et al. 2001;

✉ Ulrich A. Glasmacher
ulrich.a.glasmacher@geow.uni-heidelberg.de

Extended author information available on the last page of the article

Oehler et al. 2005; Boulesteix et al. 2013; Marques et al. 2019). The rapid mass movement can be triggered by earthquakes, new volcanic eruptions, tectonic activities, instabilities of the volcanic rock pile or a significant increase in precipitation due to climate change.

By applying luminescence dating, the deposition age of a landslide mass can be dated up to an average of 100 ka. Electron spin resonance dating of landslide masses would extent the dating possibility to about 2 Ma. Elder mass movements still seek for dating techniques. In volcanic areas, the surface of landslide remnants was covered again by volcanic flows. Dating those younger volcanic flows by applying K–Ar, $^{40}Ar/^{39}Ar$ or U/Pb techniques allowed receiving a minimum age for the mass movement (Marques et al. 2019).

In the cases of giant mass movements, resulting in the abrupt denudation of more than 2000 m of vertical material, initial rock temperatures of the suddenly exposed basal rocks drop instantaneously from high temperatures to temperatures expected on or in proximity to the Island surface. The initial rock temperature varies in dependency of thermal gradient. In active volcanic islands, a thermal gradient of more than 80 °C/km can be reached (IGME 1991a; b; Santamarta and Expósito 2014; Carlino 2018).

Such instantaneous drops in rock temperature can be recognised by applying low temperatures thermochronological (LTT) dating techniques, such as apatite and zircon fission-track and (U–Th)/He analysis. Helium diffusion in apatite is sensitive in the *T*-range of 45 °C/1 Ma to 75 °C/1 Ma; Apatite fission-tracks anneal in the *T*-range of 60 °C/10 Ma–110 °C/10 Ma; helium diffusion in zircon is sensitive to 50 °C/1 Ma to 185 °C/1 Ma depending on the amount of amorphisation, and Zircon fission-tracks anneal in the *T*-range 190 °C/10 Ma to 330 °C/10 Ma depending on the amount of amorphisation as well. Annealing and diffusion means that the revealed ages are getting younger as longer apatite and zircon are geologically kept in the specific temperature range. A sudden drop in temperature below the lower temperature of the temperature range, therefore, will freeze the system and the age received will date the sudden drop in temperature. Applying the four thermochronometers in one sample will provide the temperature decrease over more than 200 °C. To reveal the related time–temperature history of the apatite and zircon minerals and, therefore, to the rocks they have been taken from, the LTT ages are combined with numerical modelling of the time (*t*)–temperature (*T*)-evolution. In the case of giant landslides on volcanic islands, such LTT data sets derived from nowadays exposed basal volcanic, intrusive, and sedimentary units below the former > 2000 m high volcanic edifices which provide the ability to reconstruct a possible rapid cooling event from formation, or rather deposition to surface exposure.

To test the low-temperature thermochronological tools as an approach to date the rapid drop in rock temperature on volcanic islands, we chose the volcanic islands Fuerteventura and La Gomera of the Canary Archipelago. In the northern and central part of Fuerteventura Island, the nowadays exposed "Basal Complex" rock units are discussed as unravelled by giant landslides from more than 2000–3000 m high volcanic edifices (Stillman 1999; Fig. 1) in Miocene time. The Puerto Rosario debris avalanches have been formed by

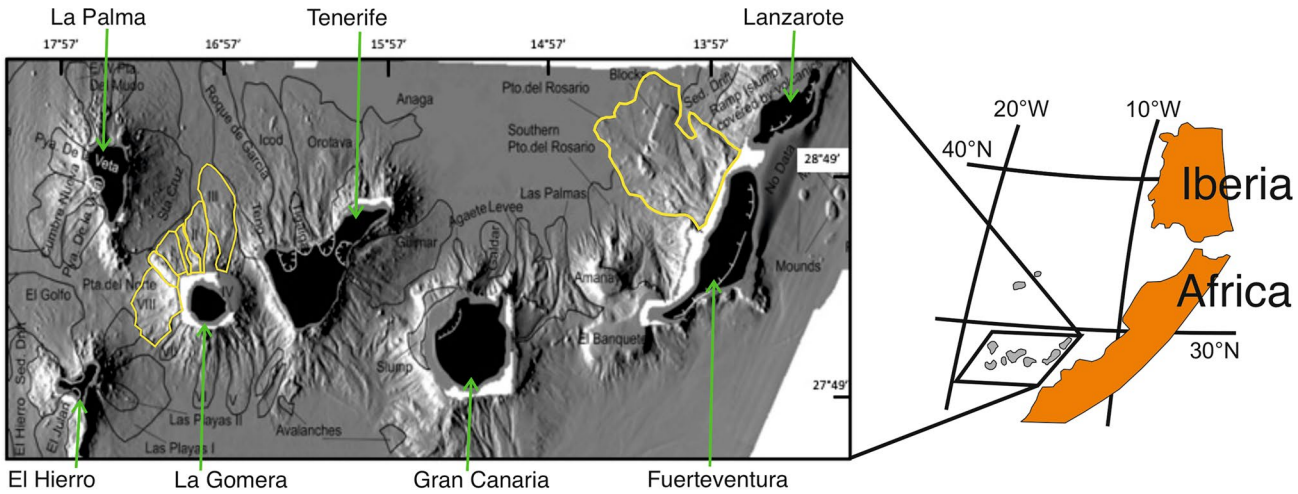

Fig. 1 Location map for the Canary Islands with respect to Africa and Iberia. Shaded relief map of the Canary Island Archipelago. The map shows the distribution of the landslides on the flanks of the Islands. Special emphasis is given to Fuerteventura and La Gomera. LRM: low relief mounds. (Shaded relief map taken from Acosta et al. (2003); slightly changed). Yellow lines encircle submarine debris avalanches that are important for this study. The submarine debris avalanche VIII and I might have partly been caused by the Tazo landslide and the submarine debris avalanche II and III might have partly been caused by the Garajonay caldera collapse and followed landslides

landslides since 20 Ma (Acosta et al. 2003; Casillas et al. 2011).

In addition, large landslides have been described and partly dated from the Canary Archipelago by Holcomb and Searle (1991), Watts and Masson (1995), Carracedo (1996), Masson (1996), Urgeles et al. (1997, 1998, 1999), Elsworth and Day (1999), Krastel et al. (2001), Masson et al. (2002), Acosta et al. (2003), Lee (2009), Casillas et al. (2008a, b, 2010), Boulesteix et al. (2013) and Coello-Bravo et al. (2020) (Fig. 1).

The northern part of La Gomera Island also exposes its "Basal Complex" because of the abrupt denudation of at least 1,300 m to 1900 m vertical rock volume of its volcanic edifice (Cendrero 1970). The exhumation age of the "Basal Complex" is assumed to have occurred several times between 12.1 and 6.4 Ma leading to the formation of the onshore and offshore Tazo, San Marcos, and other avalanches (Acosta et al. 2003; Ancochea et al. 2006; Casillas et al. 2008b, 2010; Fernández et al. 2015).

In the following, we present evidence for dating of rapid mass movements using LTT-dating techniques combined with numerical modelling. We integrate published formation ages, LTT data, and provide viable thermal histories of the "Basal Complex" of Fuerteventura and La Gomera.

Geologic setting

The Canary Archipelago is located 100–700 km west of Morocco (28.1°N latitude) in front of the Eastern Central Atlantic passive margin (Fig. 1). The seven Islands are commonly separated into (1) an internal group comprising Fuerteventura and Lanzarote, which exhibit a sub-parallel NNE–SSW alignment to the African coast, and (2) an external group, comprising the Islands El Hierro, La Gomera, La Palma, Tenerife, and Gran Canaria, which exhibit an E–W alignment. The internal group called "Eastern Canary Ridge" also comprises the submarine Conception Bank to the north and the Amanay and Banquete edifices to the south (Uchupi et al. 1976; Anchochea et al. 1996). The geological evolution of the Islands has been changed over time.

(1) A hot spot theory (plume related) was originally proposed by Burke and Wilson (1972), Schmincke (1973), Hoernle and Tilton (1991) and Hoernle and Schmincke (1993).

(2) The differences in regional distribution of the Islands have been taken as an argument against the old hot spot theory. Anguita and Hernán (1975), Araña and Ortis (1991) and Ancochea et al. (1996) assume an alternative formation model of the volcanic rocks as a "fracture-induced decompression melting of the asthenosphere". Their model connects to Alpine tectonics and is proposed to have propagated from the adjacent Moroccan Atlas Mountains towards the west.

(3) The latest theory on the origin of the Islands reassessed the plume related theory by Carracedo et al. (1998), Hoernle et al (2002), Fullea et al. (2015), Miller et al. (2015), Sagan (2018), Sagan et al. (2020) and Carnevale et al. (2021). They explain the differences to "normal hot-spot-related volcanic zones" as caused by smaller volumes of magma and eruption rates and slow motion of the related plate. Stable and radiogenic isotope data support this theory (Hoernle and Tilton 1991; Demény et al. 1998, 2004; Hoernle et al. 2002; Abu El-Rus et al. 2006).

Surface lithology on the Islands exposes volcanic and sedimentary rocks that are partly covered by sediments of Cenozoic to recent age (Fúster et al. 1968; Coello et al. 1992; Ancochea et al. 1996, 2006). The exposure of a Basal Complex (BC) on Fuerteventura and La Gomera exhibits a speciality and allows a view into the early formation stage of both Islands.

(4) Recently, the existence of seamounts in the Canary Islands environment (van den Bogaard 2013) of various ages, since the Cretaceous, have questioned the theory of the hot spot and point (Sagan et al. 2020) towards edge-driven convection (King and Anderson 1998) as the origin of Mesozoic and Cenozoic magmatism in the eastern Atlantic Ocean.

Fuerteventura Island

The geological evolution of Fuerteventura is divided in four main stages (Fig. 2; Table 1): (A) a "Mesozoic oceanic crust with sedimentary rocks"; (B) the "Eocene–Oligocene Submarine and Transitional Volcanic Group and Intrusions"; (C) a "Miocene "Subaerial Volcanic Complexes and Intrusions" comprised in series I of Fúster et al. (1968); and (D) a "Pliocene–Quaternary sedimentary and volcanic complex" comprised in series II–IV of Fúster et al. (1968). Stage A, B, and part of C also comprise the so called "Basal Complex", a term used for all exposed Mesozoic sedimentary rocks, submarine volcanic rocks, intrusive rocks, and magmatic dikes. Stage B is often separated into the "Submarine Volcanic Group" and the "Transitional Volcanic Group". The classification in Series I–IV is given by Fúster et al. (1968). The classification of A1–A4 is provided by Balogh et al. (1999). The latest classification in EM1–EM4 is published by Muñoz et al. (2003).

The following geological description is based on Bravo (1964), Fúster and Aguilar (1965), Rothe (1968), Abdel Monen et al. (1971), Robertson and Stillman (1979a, b), Fúster et al. (1980), Robertson et al. (1982), Stillman et al. (1975, 1987), Féraud et al. (1985), Le Bas et al. (1986), Ibarrola et al. (1989a, b), Coello et al. (1992), Renz et al. (1992), Cantagrel et al. (1993), Ancochea et al. (1996), Sagredo et al. (1996), Steiner et al. (1998), Balogh et al. (1999), Gutiérrez (2000), Ignacio de et al. (2002), Muñoz et al. (2005), Gutiérrez et al. (2006), Fernández et al. (2006),

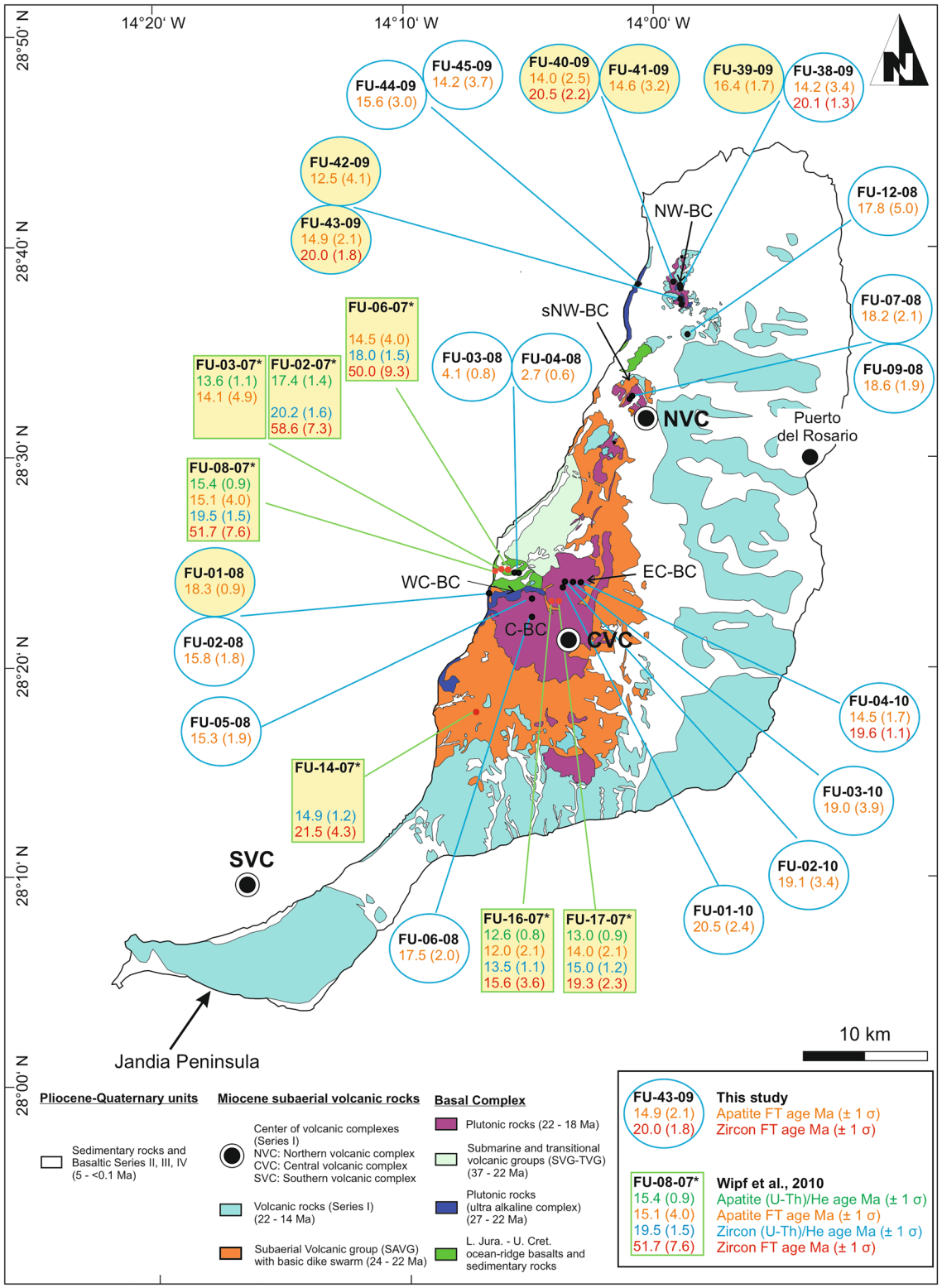

Fig. 2 Geological map of Fuerteventura Island showing the spatial distribution of the main rock units (modified after Fernández et al. 2006). Also shown are the sample locations and the determined thermochronological ages. Samples with yellow background were numerically modelled. *NW-BC* Northwest Basal Complex, *sNW-BC* southern Northwest Basal Complex, *C-BC* Central Basal Complex, *WC-BC* West-Central Basal Complex, *EC-BC* East-Central Basal Complex

Table 1 Summary of the four sedimentary, erosional, and magmatic evolutionary stages (A–D) of Fuerteventura Island partly related to the three "Volcanic Complexes" with integration of the new age data (* age data) and interpretations

Age (Ma)	Events
Stage E) Pliocene–Quaternary Sedimentary and Volcanic Complex (series II–IV of Fúster et al. 1968)	
< 0.1	Series IV: basalts + sediments + caliche
Av. 0.8–0.4	Series III: basalts + sediments
Av. 1.8–1.7	Series II: basalts + sediments and sedimentary rocks
Av. 2.9–2.4	Series II: basalts + sediments and sedimentary rocks
Av. 5	Series II: basalts + sediments and sedimentary rocks
Stage C) Miocene Subaerial Volcanic Complexes (series I of Fúster et al. 1968), and intrusions	
Northern Volcanic Complex (NVC)	
Av. 13.6 ± 0.8	**NVC II**: basalts + 20 vol.% trachybasalts + 18 vol. % trachyandesites
*~ 15	Erosional unconformity: caused by a **giant landslide** (see new data)
18.7 ± 0.3–15.3 ± 1.3	**NVC I**: basalts + 21 vol.% trachybasalts + 7 vol. % trachyandesites, trachytic dome
*18.7 ± 0.3	**NVC I**: Tindaya trachytic dome (AFT age)
Av. 18	**A3-A4 rock group** ("**Northwest Basal Complex"**): gabbros, pyroxenites
Central Volcanic Complex (CVC)	
Av. 15.1 ± 0.5	**CVC III**: basalts + 35 vol.% trachybasalts
*~ 16	Erosional unconformity: caused by a **giant landslide**
*19.6 ± 1.1	**CVC II**: subaerial lava flow (ZFT age)
Av. 20.8 ± 0.8	**CVC II**: basalts + 10 vol.% trachybasalts + 3 vol. % trachyandesites + trachyte
*~ 20	Erosional unconformity: caused by a **giant landslide**
18.7 ± 0.8–16.05 ± 0.04	*A4, EM3, EM4 rock group **("East-Central Basal Complex")**: gabbros, syenites*
> 21.5 ± 0.8	**CVC I**: basalts + 7 vol.% trachyandesites
Southern Volcanic Complex (SVC)	
*	Erosional unconformity (caused by **landslide**)
Av. 14.7 ± 0.5	**SVC III**: basalts + 20 vol.% trachybasalts
*	Erosional unconformity (caused by **landslide**)
Av. 16.8 ± 0.4	**SVC II**: basalts + 10 vol.% trachybasalts
*	Erosional unconformity (caused by **landslide**)
Av. 20.7 ± 0.4	**SVC I**: basaltic volcanic rocks
Initial Miocene Subaerial Volcanic Group (SAVG) with basic dike swarm	
24–22	Subaerial Volcanic Group (SAVG): lava flows and pyroclastics (basalts, trachybasalts)
*21.5 ± 4.3	N–S trending dike **N of Montaña Sicasumbre** ***("West-Central Basal Complex")*** (ZFT age)
22.10 ± 0.07–21.8 ± 0.5	*A3, EM2 rock group **("West-Central Basal Complex")**: gabbros, pyroxenites*
Miocene	N–S trending basic dike swarm (coeval with generation of SAVG)
Stage B) Eocene–Oligocene Submarine and Transitional Volcanic Group and intrusions	
U. Oligocene–Miocene	Basaltic submarine-subaerial lava flows ***("West-Central Basal Complex")*** (SVG-TVG)
36.3 ± 1.7–26.9 ± 1.0	*A2, EM1 rock group **("Northwest Basal Complex")**: alkali pyroxenites, amphibole gabbros, carbonatites, syenites*
26.7 ± 1.1–22.1 ± 1.3	*A2, EM1 rock group **("West-Central Basal Complex")**: alkali pyroxenites, amphibole gabbros, carbonatites, syenites*
Oligocene	Pillow lavas, hyaloclastites, basaltic volcanic breccias ***("West-Central Basal Complex")*** (SVG)
Stage A) Mesozoic oceanic crust with sedimentary rocks	
Lower Jurassic–Upper Cretaceous	Deep-water sedimentary sequence
Lower Jurassic	Tholeiitic N-type mid-ocean-ridge basalts

Old age data are taken from published literature (see this publication)

S.V.G. Submarine Volcanic Group, *ZFT age* zircon fission-track age, *AFT age* apatite fission-track age, *T.V.G.* Transitional Volcanic Group; *Italic = domes, intrusions or dikes*. Series I–IV: Fúster et al. (1968), A1–A4: Balogh et al. (1999), EM1–EM4: Munoz et al. (2003). The transfer of radiometric ages into stratigraphic ages used the International Chronostratigraphic Chart version 2022/02 of the International Commission on Stratigraphy (Cohen et al. 2013)

Casillas et al. (2008a) and Allibon et al. (2011a, b). The transfer of radiometric ages into stratigraphic ages used the International Chronostratigraphic Chart version 2022/02 of the International Commission on Stratigraphy (Cohen et al. 2013).

Stage A, B, and part of C: the "Basal Complex" (Early Jurassic to Miocene)

The "Basal Complex" is exposed in the Northwest ("Northwest Basal Complex": NW-BC) and Central part ("Central Basal Complex": C-BC) of Fuerteventura. In the northwest of the Island, the Basal Complex is partly overlain by the volcanic rocks of the Northern Volcanic Complex (NVC, Series I) and sediments and sedimentary rocks of the "Pliocene to Quaternary Sedimentary and Volcanic Complex". The "Central Basal Complex" is partly overlain by volcanic rocks of the Central Volcanic Complex (CVC, Series I) and volcanic and sediments and sedimentary rocks of the "Pliocene to Quaternary Sedimentary and Volcanic Complex" (Series II–IV). We separated the "Central Basal Complex" into a "West- and East-Central Basal Complex": The "West-Central Basal Complex" extends from the Atlantic Ocean to Vega de Rio Palmas. The "East-Central Basal Complex" extends from Vega de Rio Palmas to the Betancuria.

The Mesozoic oceanic crust of the "Basal Complex" consists of tholeiitic N-type mid-ocean-ridge basalts of Lower Jurassic age (Toarcium, Steier et al. 1998) overlain by a thick deep-water sedimentary sequence of Lower Jurassic to Upper Cretaceous age. The formation age of the sedimentary sequence is well constrained by paleontological evidence (Renz et al. 1992; Steiner et al. 1998). Oligocene pillow lavas, hyaloclastites, basaltic volcanic breccias of the "Submarine Volcanic Group" (SVG), the submarine growth stage of Fuerteventura, unconformable overlie the Mesozoic sedimentary sequence. The Upper Oligocene basaltic submarine-subaerial lava flows of the "Transitional Volcanic Group" (TVG), which corresponds to the emergence stage of the island follow the "Submarine Volcanic Group". Numerous small plutonic and hypabyssal intrusions occur within the Mesozoic to Cenozoic bedded succession. Crosscutting relationships led to recognise four intrusive episodes for the "Basal Complex" [if not stated otherwise all ages of the rock groups A1–A3 are $^{40}Ar/^{39}Ar$ mineral ages or whole rock ages (wr)], AFT = apatite fission-track age (Ignacio de et al. 2002):

- *A1 or EM1 rock group* (occur only in the "West-Central Basal Complex"): alkali pyroxenites, amphibole gabbros, and syenites (wr $^{40}Ar/^{39}Ar$ ages: 23.5 ± 1.0 Ma–70.6 ± 3.9 Ma). Feldspar (fsp) and nepheline separated from one syenite provided $^{40}Ar/^{39}Ar$ ages of 63.1 ± 0.8 Ma and 64.2 ± 1.0 Ma which are interpreted as the syenite intrusion age. These ages are within error the same as the whole rock (wr) age of one pyroxenite (64.7 ± 3.2 Ma). Ages younger ages than ~ 64 Ma are interpreted as thermal alteration of the $^{40}Ar/^{39}Ar$-system and ages older as ~ 64 Ma are caused by excess argon.
- *A2 or EM1 rock group* ("Northwest Basal Complex"): *Las Montanetas Complex:* carbonatite fsp = 27.7 ± 1.2 Ma; *Barranco de Agua Salada Complex:* carbonatite phlogopite (ph) = 26.9 ± 1.0 Ma; *Los Jablitos Complex:* carbonatite ph = 28.1 ± 4.3 Ma, syenite fsp = 30.9 ± 1.2 Ma; perovskite–clinopyroxenite K–Ar wr = 26.2 ± 3 Ma; *Barranco de Esquinzo Complex:* syenite fsp = 36.3 ± 1.7 Ma also indicate Oligocene to Miocene intrusion ages.
- *A2 or EM1 rock group* ("West-Central Basal Complex"): *Punta Penón Blanco Complex:* carbonatite fsp = 24.0 ± 0.9 Ma; biotite (bio) = 22.7 ± 0.9 Ma, syenite wr = 22.1 ± 1.3 Ma; *Caleta de la Cruz Complex:* carbonatite bio = 23.8 ± 1.0 Ma, syenite wr = 26.7 ± 1.1; indicate Oligocene to Miocene intrusion ages.
- *A3 or EM2 rock group* ("Northwest Basal Complex"): *Montaña Blanca-Milocho*: nepheline-bearing amphibole-gabbro K–Ar wr: 26.7 ± 1.2 Ma AFT = 25.4 ± 3.6 Ma and 29.3 ± 3.5 Ma; ("West-Central Basal Complex"): Various NNE–SSW elongated Early Miocene gabbro and pyroxenite bodies comprises the third group (23 Ma–22 Ma). Pajara Pluton PX1 (U–Pb age zircon, baddeleyite = 22.10 ± 0.07 Ma; $^{40}Ar/^{39}Ar$ ages amphibole = 21.9 ± 0.6 to 21.8 ± 0.3 Ma
- *A4 or EM3 rock group* ("East-Central Basal Complex"): Gabbros and syenites of the Vega de Rio Palmas Ring Complex (fourth unit; U–Pb ages of zircon: syenites = 18.7 ± 0.8 Ma–16.05 ± 0.04 Ma; gabbro 18.4 ± 0.3 Ma–17.16 ± 0.40 Ma) and the Betacuria Complex (A4, EM 4; unknown age) form the youngest intrusive unit.

K/Ar ages are based on Abdel Monen et al. (1971), Féraud et al. (1985), Le Bas et al. (1986), Ibarrola et al. (1989a), Cantagrel et al. (1993), Sagredo et al. 1996), Balogh et al. (1999), Ignacio de et al. (2002), and Gutiérrez et al. (2006). $^{40}Ar/^{39}Ar$ age data are published by Féraud et al. (1985), Balogh et al. (1999), and Gutiérrez et al. (2006). U–Pb ages of zircon are taken from an internal report of Casillas (2022).

Stage C: Miocene volcanic complexes and intrusions (series I)

The volcanic rocks (lava flows and pyroclastic rocks: basalts, trachybasalts) of the initial subaerial volcanic eruptions are summarised in the Miocene Subaerial Volcanic Group (SAVG) as the first subaerial eruptions around 24–22 Ma. Coeval to the SAVG is the Miocene N–S trending basic dike swarm (23–17 Ma) that occur in the "Basal Complex". The

initial volcanic activity is followed by eruptions building the three Volcanic Complexes on Fuerteventura Island, the southern, central, and northern volcanic edifice. The Volcanic Complexes that reach a maximum elevation of about 3000 m display a heterogeneous series of basalts, trachybasalts, debris avalanche breccias, and debris flow breccias that are crosscut by dikes and plutonic bodies of unknown age. All ages are either K–Ar ages or $^{40}Ar/^{39}Ar$ ages of whole rock or minerals.

The Southern Volcanic Complex (SVC) consists of three dated volcanic stages (SVC I: av. 20.7 ± 0.4 Ma, SVC II: base av. 16.8 ± 0.4 Ma to top av. 15.7 ± 0.3 Ma, SVC III: av. 14.7 ± 0.5 Ma; separated by erosional unconformities assumably caused by landslides. The remains of the Central Volcanic Complex (CVC) also consist of three volcanic stages separated by erosional unconformities (CVC I: older than 21.5 ± 0.8 Ma; CVC II: av. 20.8 ± 0.8 Ma; CVC III: av. 15.1 ± 0.5 Ma). The Northern Volcanic Complex (NCV) exhibit two volcanic stages: the NVC I (18.7 ± 0.3 Ma–15.3 ± 1.3 Ma) and the NVC II av. 13.6 ± 0.8 Ma).

In the core of the Northern and Central Volcanic Complexes, the hypabyssal root of successive growth occurs as a series of plutonic rocks (pyroxenites, gabbro's, syenites, basaltic to trachybasaltic dykes; equivalent to the intrusive periods three to four of the "Basal Complex"). K/Ar ages are based on Abdel Monen et al. (1971), Féraud et al. (1985), Coello et al. (1992), and Ancochea et al. (1996). $^{40}Ar/^{39}Ar$ age data are published by Féraud et al. (1985).

Stage D: Pliocene–Quaternary sedimentary and volcanic complex (series II–IV)

The post-Miocene volcanism on Fuerteventura occurred only in the Central and Northern regions of the island, producing eruptive cycles with K/Ar ages of ~ 5 Ma, 2.9–2.4 Ma, 1.8–1.7 Ma, 0.8–0.4 Ma, and < 0.1 Ma. Renewed activity formed small basaltic volcanoes and associated lava fields during the Pliocene that continued until the prehistoric. Series II comprises three periods of volcanic activity during the Lower Pliocene, Upper Pliocene, and at the Pliocene–Pleistocene boundary; series III crops out in a few localities of Pleistocene age; and series IV ranges from Upper Pleistocene to Holocene. Littoral and shallow-water marine deposits, aeolian and alluvial complexes and paleosol deposits are formed during the Pliocene–Quaternary period (Abdel Monen et al. 1971; Ibarrola et al. 1989a, b; Coello et al. 1992; Ancochea et al. 1996).

La Gomera Island

La Gomera comprises a single, very large Volcanic Complex (24 km in diameter) formed by three main evolutionary phases (Bravo 1964; Cendrero 1971; Cubas 1978; Ancochea et al. 2006; Fernández et al. 2015; Márquez et al. 2018; Fig. 3; Table 2):

- The Basal Complex comprises the submarine volcanic stage and intrusions (12.1 ± 0.1–9.0 ± 0.5 Ma).
- The Old Edifice (10.8 ± 2.4–6.4 ± 0.5 Ma) separated into a Lower Old Edifice (10.8 ± 2.4–8.7 ± 0.4 Ma)) and an Upper Old Edifice (10.5 ± 0.2–6.4 ± 0.5 Ma).
- The Young Edifice (5.7 ± 0.3–2.8 ± 0.1 Ma) that comprises the Young Edifice-1 and the Young Edifice-2 (Fig. 3).

Like Fuerteventura, a rapid exhumation caused by landslides (flank failure) have occurred in Miocene time. In both cases, remnants of the giant landslides have been studied in detail (Casillas et al. 2008a, 2010). La Gomera has experienced no volcanic activity in the last 2 Myr (Million years), and thus, represents an exceptional case in the Canary Islands (Márquez et al. 2018). The following geological description is based on Cendrero (1970, 1971), Abdel Monen et al. (1971), Cantagrel et al. (1984), Cubas et al. (1994), Ancochea et al. (2003, 2006, 2008), Herrera et al. (2008), Casillas et al. (2008b, c, 2010), Demény et al. (2010), Fernández et al. (2015) and Márquez et al. (2018). The transfer of radiometric ages into stratigraphic ages used the International Chronostratigraphic Chart version 2022/02 of the International Commission on Stratigraphy (Cohen et al. 2013).

Miocene submarine volcanic stage and intrusions (12.1 ± 0.1–9.0 ± 0.5 Ma)

As in Fuerteventura, in La Gomera, the term "Basal Complex" is used for a suite of different sedimentary, volcanic, and intrusive rocks. The "Basal Complex", which exposed at the NW part of the island, is formed by siliciclastic and carbonatic sedimentary rocks (older than 20 Myr), Miocene submarine volcanic rocks (pillow lavas, trachytic breccias), and ultramafic to mafic intrusions of Miocene age. The P1 suite consists of kaersutite pyroxenite, kaersutite, and amphibole-gabbro intrusions. All BC rocks are cut by an extremely dense network of basic dikes and are markedly deformed. The published K/Ar and $^{40}Ar/^{39}Ar$ age data suppose a formation age between 11.5 ± 0.7 and 8.9 ± 0.1 Ma for the rocks of the "Basal Complex". K/Ar ages are based on Abdel Monen et al. (1971), Cantagrel et al. (1984), Cubas et al. (1994) and Anchochea et al. (2003, 2006). $^{40}Ar/^{39}Ar$ age data are published by Herrera et al. (2008).

The Old Edifice (OE; Upper Miocene; 10.8 ± 2.4–6.4 ± 0.5 Ma)

The Subaerial Volcanic Stage of La Gomera Island started at about 10.8 Ma with the formation of the Old Edifice. The

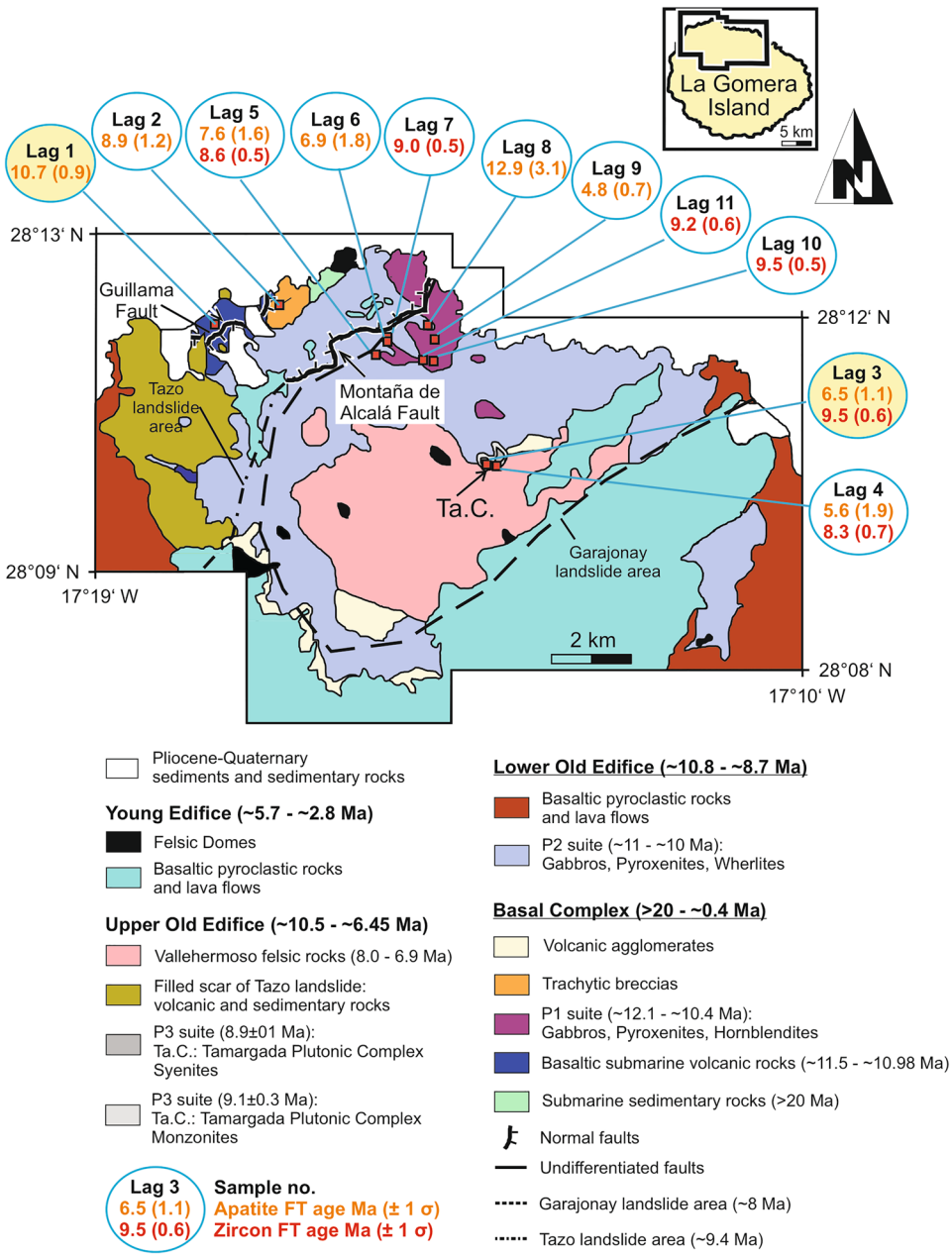

Fig. 3 Geologic map of the northern sector La Gomera Island showing the distribution of the main rock units, the locations of the dated samples, and the thermochronological ages. The inset shows the area covered by the map from La Gomera (modified after Casillas et al. 2010). The outline of the possible Garajonay landslide was taken from Paris et al. (2005). Samples with yellow background were numerically modelled. Ta.C. Tamargada Complex

Lower Old Edifice is represented by a monotonous accumulation of Pahoehoe basaltic lava flows with rare interspersed basaltic pyroclastic layers deposited between 10.8 ± 2.4 Ma and 8.7 ± 0.4 Ma [whole rock (wr): K/Ar ages]. The P2 suite consists of clinopyroxenite, wehrlite, gabbros, and olivine gabbro intrusion (10.8 ± 0.1–10.6 ± 0.1 Ma). The centre of the Lower Old Edifice would have reached a height between 1300 and 1900 m. Between 8.6 ± 0.4 Ma and 8.0 ± 0.3 Ma (wr: K/Ar ages) the lower part of the Upper Old Edifice covers the partially destroyed Lower Old Edifice. The P3 suite consists of alkaline gabbro, monzodiorite, and syenite intrusions. Famous is the Tamargada monzonite–syenite complex (9.1 ± 0.3 Ma, 8.9 ± 0.1 Ma, respectively). The upper most unit, the Upper Old Edifice-2 of basaltic and trachybasaltic flows and dikes cover the age range between 7.5 ± 0.4 Ma and 6.5 ± 0.3 Ma. The Upper Old Edifice reached a final height of about 2200 m. Associated with the Old Edifice is a cortege of felsic intrusive rocks, the Vallehermoso trachytic-phonolitic complex with a K/Ar whole rock age range from 8.6 ± 0.4 to 6.4 ± 0.5 Ma. The Tamargada syenite revealed

Table 2 Sedimentary, erosional, and magmatic evolution of La Gomera Island

Age (Ma)	Events
Miocene–Pliocene Subaerial Volcanic Stage and intrusions (Young Edifice)	
4.6 ± 0.1–2.8 ± 0.1	Young Edifice-2: basaltic + trachybasaltic + trachyandesitic + trachytic lava flows
4.5 ± 0.2–4.0 ± 0.2	*Young Edifice-2: basaltic + trachybasaltic dikes*
4.5 ± 0.2–4.3 ± 0.1	*Young Edifice-2: trachytic + phonolitic domes*
5.7 ± 0.3–5.6 ± 0.1	Young Edifice-1: basaltic lava flows,
5.5 ± 0.3–4.7 ± 0.2	*Young Edifice-1: basaltic + trachybasaltic dikes*
5.1 ± 0.3–4.6 ± 0.3	*Young Edifice-1: trachytic + phonolitic domes*
Miocene Subaerial Volcanic Stage and intrusions (Old Edifice)	
*~ 6.5	Erosional unconformity: caused by a landslide (see new data)
8.6 ± 0.4– 6.5 ± 0.3	**Upper Old Edifice**: basaltic + trachybasaltic lava flows and dikes
8.0 ± 0.4	*Trachytic to phonolitic dikes*
8.6 ± 0.4– 6.4 ± 0.5	*Vallehermoso trachytic-phonolitic complex*
*~ 9	Erosional unconformity: caused by the Tazo landslide (see new data)
10.5 ± 0.2–8.1 ± 0.5	Basaltic dikes *(1 every 10 m)*
**8.3 ± 0.7*	*Tamargada syenite (ZFT age)*
**9.5 ± 0.6*	*Tamargada monzonite (ZFT age)*
9.1 ± 0.3– 8.9 ± 0.1	*P3 suite: Tamargada complex (monzonite-syenite)*
10.8 ± 2.4–8.7 ± 0.4	**Lower Old Edifice:** Pahoehoe basaltic lava flows + rare interspersed basaltic pyroclastic layers
	NW–SE, N–S trending basic dike swarm
10.8 ± 0.1– 10.6 ± 0.1	*P2 suite: clinopyroxenite, wehrlite, gabbros, olivine gabbros*
~ 10.8	Start of Subaerial Volcanic Stage
Miocene submarine Volcanic Stage and intrusions ("Basal Complex")	
**9.0 ± 0.5*	*P1 suite: amphibole gabbros (ZFT age)*
**9.5 ± 0.5*	*P1 suite: trachyte dike (ZFT age)*
12.1 ± 0.1–10.4 ± 0.2	***P1 suite:** hornblende pyroxenites, hornblendite, amphibole gabbros*
11.5 ± 0.7– 10.98 ± 0.08	Pillow lavas, hyaloclastites, basaltic volcanic breccias
Sedimentary rocks (Basal Complex)	
> 20 Ma	Siliciclastic and carbonatic sedimentary sequence

Age data are taken from Abdel Monen et al. (1971), Cantagrel et al. (1984), Cubas et al. (1994), Anchochea et al. (2003, 2006, 2008), and Herrera et al. (2008)

*Age data = new data of this publication. (Abbreviations see text; *Italic = domes, intrusions or dikes*). The transfer of radiometric ages into stratigraphic ages used the International Chronostratigraphic Chart version 2022/02 of the International Commission on Stratigraphy (Cohen et al. 2013)

a K/Ar whole rock age of 9.1 ± 0.3 Ma and a whole rock $^{40}Ar/^{39}Ar$ age of 8.5 ± 0.2 Ma. The Old Edifice rock units are characterised by intense interaction of crosscutting dykes (1 every 10 m or even less) of basaltic composition (10.5 ± 0.2–8.1 ± 0.5 Ma) and less frequent felsic (trachytic to phonolitic) ones (8.0 ± 0.4 Ma). K/Ar ages are based on Abdel Monen et al. (1971), Cantagrel et al. 1984, Féraud et al. (1985) and Anchochea et al. (2006, 2008). $^{40}Ar/^{39}Ar$ age data are published by Herrera et al. (2008).

The Young Edifice (YE, Upper Miocene to Pliocene (5.7 ± 0.3–2.8 ± 0.1 Ma)

The Young Edifice comprises more than 1000-m-thick series of lava flows, pyroclastic rocks intruded by domes, and crossed by dikes. The Young Edifice can be divided into a Young Edifice-1 (YE-1) and a Young Edifice-2 (YE-2). The Young Edifice-1 comprises basaltic lava flows from the central region

of La Gomera descending towards the south and southwest, basaltic and trachybasaltic dikes and trachytic and phonolitic domes of 5.7 ± 0.3–4.7 ± 0.2 Ma. The Young Edifice-2 contains widespread sub-horizontal and broad detached basaltic + trachybasaltic + trachyandesitic + trachytic lava flows (4.6 ± 0.1–2.8 ± 0.1 Ma) extending to the North-, West-, and Northeast-margins of the island. Ages are based on Abdel Monen et al. (1971), Féraud et al. (1985), and Anchochea et al. (2008).

Methodology

Sample description

21 magmatic rocks of Fuerteventura Island and 11 magmatic rocks of La Gomera Island of different formation ages were sampled with the aim to determine extrusion ages and generate the history from intrusion or extrusion to the recent surface position. In addition, we integrated and reinterpreted thermochronological data of seven magmatic and sedimentary rock samples published by Wipf et al. (2010). Furthermore, by applying annealing and diffusion kinetics using the software code HeFty (version 1.9.3) the concept of giant landslides published by Stillman (1999), and others see "Introduction" (Fig. 1; Tables 3, 4) was tested against the thermochronological data set. The intrusive and dike rock samples of Fuerteventura cover all lithologies and the different stratigraphic units (A1–A4; EM 1, EM 3, EM 4) of the "Northwest Basal Complex" and the "Central Basal Complex".

Samples of the "Northwest Basal Complex" are two carbonatite dikes (#FU-38-09, Form. age: 27.7 ± 1.2 Ma; #FU-40-09, Form. age: 27.2 ± 0.4 Ma), two pyroxenites (#FU-39-09, Form. age: unknown), two Ijolites (#FU-41-09, Form. age: 27.3 ± 0.5 Ma; #FU-44-09, Form. age: 27.3 ± 0.5 Ma), and two syenite dikes (#FU-43-09, Form. age: 27.3 ± 0.6 Ma; #FU-45-09, Form. age: 28.3 ± 0.2 Ma) (Fig. 2). One layered and one coarse-grained gabbro of unknown formation age were sampled in the "southern Northwest Basal Complex".

Lithologies and stratigraphic units of the West-Central Basal Complex are represented by three Lower cretaceous sandstones (#FU-02-07*, #FU-06-07*, #FU-08-07*, Form. age: 137–112 Ma), three basic dikes (#FU-03-07*, #FU-14-07*, #FU-06-08, Form. age: 24–17 Ma), two syenite dikes (#FU-02-08, #FU-05-08, Form. age: 26.2 ± 0.2 Ma), and one carbonatite dike (#FU-01-08, Form. age: 26.2 ± 0.2 Ma).

Three syenite samples partly coarse-grained (#FU-16-07*, Form. age: 18.7 ± 0.8 Ma, #FU-01-10, Form. age: unknown, #FU-03-10, Form. age: unknown), one gabbro (#FU-17-07*, Form. age: 18.4 ± 0.3 Ma), and one trachyte (#FU-02-10, Form. age: unknown) are taken from the East-Central Basal Complex.

One trachyte sample (#FU-12-08, Form. age: 18.7 ± 0.3 Ma) was taken from the Tindaya trachytic dome that belongs to the Northern Volcanic Complex series I. The Central Volcanic Complex series I is represented by one subaerial basic lava (#FU-04-10, Form. age: 20–21 Ma).

In La Gomera, the analysed samples cover the submarine volcanic rock stage, and the P1 to P3 suite (Fig. 3). The submarine volcanic rocks are represented by a pillow basalt sample (#Lag 1, Form. age: 11.5 ± 0.7 Ma), and a submarine trachytic hyaloclastite (#Lag 2, Form. age: 10.98 ± 0.08 Ma). Samples of the P1 suite consist of two amphibole gabbros (#Lag 6, Lag 7, Form. age: 10.6 ± 0.1 Ma), one amphibole pyroxenite (#Lag 10, Form. age: 12.1 ± 0.1 Ma), and two trachyte dikes (##Lag 9, Lag 11, Form. age: 10.4 ± 0.2 Ma and 10.7 ± 0.1 Ma, respectively). The P2 suite is represented by a syenite dike (#Lag 5, Form. age: 10.6 ± 0.1 Ma), and a pegmatitic gabbro (#Lag 8, Form. age: 10.8 ± 0.1 Ma). Samples of the Tamargada monzonite (#Lag 3, Form. age: 8.9 ± 0.1 Ma, and the Tamargada syenite (#Lag 4, For. age: 9.1 ± 0.3 Ma) belong to the P3 suite.

Thermochronology

Thermochronology is based on the accumulation and thermally controlled retention of isotopic daughter products and linear crystal defects produced during the radioactive decay of the parents. Due to the temperature sensitivity of the thermochronometers, ages provide information about the cooling history of the rock. If temperatures decrease rapidly such as it is attributed to the cooling of volcanic flows, thermochronological ages represent the formation age of the flow.

Apatite and zircon fission-track (AFT and ZFT, respectively) dating techniques were performed on 21 samples located on Fuerteventura Island (Table 3, Fig. 2) and 11 magmatic rock samples on La Gomera Island (Table 4, Fig. 3). Already published AFT, and ZFT, and (U–Th–Sm)/He (AHe and ZHe, respectively; Wipf et al. 2010) ages of seven rock samples from Fuerteventura were integrated in the discussion and for the first time the time–temperature evolution was numerical modelled.

Sample preparation and analyses followed the same protocol as, e.g. Karl et al. (2013) with the exception of the apatite etching conditions. 5.5 N HNO_3 for 20 (± 1) s at 21 (± 1) °C that was applied to all apatite mounts. We extracted suitable zircon grains for ZFT analyses from 4 new samples (Figs. 2, 3; Tables 5, 6) and suitable apatite grains for AFT dating from 21 new samples (Figs. 2, 3; Tables 5, 6). As the spontaneous track densities were generally low with values ranging from ~ 0.1 to ~ 0.7 insufficient number of confined

Table 3 Samples taken from Fuerteventura Island, analysed by apatite and/or zircon fission-track- and (U–Th)/He-dating technique

S.-no	Coordinates UTM		Elevation (m.a.s.l.)	Lithology	Formation age	Formation age (Ma)
	E	N				
Northwest Basal Complex						
A1, A2, EM1 rock group: Montaña Blanca-Esquinzo sector						
FU-38-09	28R 599292	3,168,170	177	Carb. (D)	U. Oligo.	27.7 ± 1.2 (5)
FU-39-09	28R 599168	3168009	134	Pyroxenite	–	–
FU-40-09	28R 599699	3171307	149	Carb. (D)	U. Oligo.	27.2 ± 0.4 (6)
FU-41-09	28R 599699	3171307	149	Ijolite	U. Oligo.	27.3 ± 0.5 (6)
FU-42-09	28R 599036	3166635	108	Pyroxenite	–	–
FU-43-09	28R 598866	3166793	102	Syenite (D)	U. Oligo.	27.3 ± 0.6 (6)
FU-44-09	28R 595072	3167805	3	Ijolite	U. Oligo.	27.3 ± 0.5 (6)
FU-45-09	28R 595072	3167805	3	Syenite (D)	L. Oligo.	28.3 ± 0.2 (6)
A3, A4, EM3, EM4 rock group: Southern Northwest Basal Complex						
FU-07-08	28R 593654	3156289	90	lay. Gabbro	–	–
FU-09-08	28R 595327	3167906	16	cg. Gabbro	–	–
West-Central Basal Complex						
Sedimentary rock unit: North of Ajui						
FU-02-07*	28R 582742	3143185	41	Sandstone	L. Cret.	137–112 (4)
FU-06-07*	28R 583424	3143151	40	Sandstone	L. Cret.	137–112 (4)
FU-08-07*	28R 584280	3143033	8	Sandstone	L. Cret.	137–112 (4)
Sheeted Dike Swarm unit: North of Ajui						
FU-03-07*	28R 582742	3143185	41	Basalt (sh. D)	L. Mio.	23–17 (1)
Sheeted Dike Swarm unit: North of Montaña Sicasumbre						
FU-14-07*	28R 582170	3129330	408	Basalt (sh. D)	L. Mio.	23–17 (1)
A1, A2, EM1 rock group: South of Ajui						
FU-01-08	28R 582156	3140938	0	Carb. (D)	U. Oligo.	26.2 ± 0.2 (6)
FU-02-08	28R 582156	3140938	0	Syenite (D)	U. Oligo.	26.2 ± 0.2 (6)
A3, A4, EM2, EM3 rock group: around Pajara						
FU-05-08	28R 587685	3140332	175	Syenite	–	–
FU-06-08	28R 586925	3136294	205	Basalt (D)	–	–
Unknown formation age						
FU-03-08	28R 586628	3143340	178	Trachyte (D)	–	–
FU-04-08	28R 586765	3143248	200	Trachyte (D)	–	–
East-Central Basal Complex						
A4, EM3 rock group: Vega de Rio Palmas Ring Complex						
FU-16-07*	28R 588459	3139759	318	Syenite	L. Mio.	16.05 ± 0.04 (6) 17.0 ± 0.2 (6) 18.26 ± 0.26 (6) 18.7 ± 0.8 (6)
FU-17-07*	28R 589272	3140574	318	Gabbro	L. Mio.	17.16 ± 0.40 (6) 18.4 ± 0.3 (6)
A4, EM3, EM4 rock group: South of Betancuria						
FU-01–10	28R 592080	3142246	333	cg. Syenite	–	–
FU-02–10	28R 592042	3142363	328	Trachyte	–	–
FU-03–10	28R 592376	3142371	353	cg. Syenite	–	–
Northern Volcanic Complexes series I (NVC I): Tindaya trachytic dome						
FU-12-08	28R 599602	3163325	173	Trachyte	L. Mio.	18.7 ± 0.3 (2)
Central Volcanic Complexes series I (CVC I)						
FU-04–10	28R 592423	3142338	357	subaerial Lava	L. Mio.	20–21 (2, 3)

S.-no.: sample numbers; FU-38-09: Fuerteventura-sample-year

*Represent samples analysed by Wipf et al. (2010); NVC I: Northern Volcanic Complex I; CVC II: Central Volcanic Complex II; m.a.s.l.: metre above sea level; Carb.: carbonatite; lay.: layered; cg.: coarse-grained; (D): dike; (sh. D): sheeted dike complex; Formation ages taken from (1): Feraud et al. (1985); (2): Coello et al. (1992); (3): Ancochea et al. (1996); (4): Steiner et al. 1998; (5): Balogh et al. (1999); (6): Casillas et al. (2022); U. Oligo.: Upper Oligocene; Cret.: Cretaceous; L. Mio: Lower Miocene; av.: average; –: age unknown. Series I–IV: Fúster et al. (1968), A1–A4: Balogh et al. (1999), EM1–EM4: Munoz et al. (2003). The transfer of radiometric ages into stratigraphic ages used the International Chronostratigraphic Chart version 2022/02 (Cohen et al. 2013)

fission-tracks (CTs) were etched. To reveal more CTs by artificial etchant conduits, a second set of apatite mounts was prepared from samples of Fuerteventura and La Gomera. The artificial etchant conduits are formed by the irradiation with accelerated heavy ions (Jonckheere et al. 2007), like the irradiation with fission fragments from a ^{252}Cf source (Donelick and Miller 1991). The apatite mounts were irradiated by ^{197}Au ion at the universal linear accelerator (UNILAC) facility, GSI Helmholtzzentrum für Schwerionenforschung GmbH in Darmstadt, Germany with an energy of 11.1 MeV/nucleon, a fluence of 1×10^6 ions/cm^2, and an angle of 15° with the vertical. Irradiation followed the protocol published by Jonckheere et al. (2007). After irradiation, the mounts were etched with 5.5 N HNO_3 for 20 (± 1) s at 21 (± 1) °C. After etching CTs were located within the apatite grains (Table 7).

The published apatite and zircon fission-track ages and the apatite (U–Th)/He (AHe) and zircon (U–Th)/He (ZHe) data were re-examinate and used to numerically model the time–temperature-evolution for the first time (Table 8). Re-examinate of the fission-track data means: We remeasured the confined fission-track length in old apatite grains (Wipf et al. 2010) and determined the angle of the CT to the *c*-axes of the apatite crystal. We chose the crystal size and form as the selection criterion for zircon and apatite grains for the (U–Th–Sm)/He system as it is used in such data (Brown et al. 2013; Beucher et al. 2013; Green and Duddy 2018), as well as homogeneity in grain size and chemical content [U, Th, Sm, low radiation damage (eU-value)] of used apatite and zircon grains. This was possible as the old already dated [(U–Th–Sm)/He dating] apatite and zircon grains were documented with photos. Therefore, we only present clear grains for apatite and clear, light coloured grains for zircon, respectively, when the requirement for a full morphology was fulfilled. The influence of zircon colour as a selecting criterion in fission-track dating is well described by Garver and Kamp (2002). This criterion can also be applied to ZHe-dating. In addition, since the last publication in 2010 the He-diffusion and fission-track annealing models and the knowledge on the influence of grain shape have been advanced significantly. Therefore, a re-examination and new numerical modelling of the already published data was necessary.

Mineral dating technique corresponds to a specific closure temperature (*T*(c)) and total annealing temperature (*T* (an)). When temperatures exceed *T*(c) and *T* (an) over certain time (e.g. AHe: 75° must last 1 Myr for complete loss

Table 4 Samples taken from La Gomera Island and analysed by apatite and/or zircon fission-track

S.-no	Com.	Coordinates UTM		Elev. (m.a.s.l.)	Lith.	Form. age	Form. age (Ma)
		E	N				
La Gomera Basal Complex							
Submarine volcanic rocks							
Lag 1	LG-BC	28R 273943	3121536	200	Pill.-bas.	U. Mio.	11.5 ± 0.7 (2)
Lag 2	LG-BC	28R 275033	3122075	70	Subm. Trachy. Hyalocl.	U. Mio.	10.98 ± 0.08 (3)
P1 suite							
Lag 6	LG-BC	28R 277370	3121607	310	Am.-Gab.	U. Mio.	10.6 ± 0.1 (3)
Lag 7	LG-BC	28R 277370	3121607	310	Am.-Gab.	U. Mio.	10.6 ± 0.1 (3)
Lag 9	LG-BC	28R 277985	3121869	325	Trach. (D)	U. Mio.	10.4 ± 0.2 (3)
Lag 10	LG-BC	28R 278413	3121301	75	Am.-Pyrox.	M. Mio.	12.1 ± 0.1 (3)
Lag 11	LG-BC	28R 278279	3121289	65	Trach. (D)	U. Mio.	10.7 ± 0.1 (3)
P2 suite							
Lag 5	Lower Old Edifice	28R 277348	3121333	280	Sy. (D)	U. Mio.	10.6 ± 0.1 (3)
Lag 8	Lower Old Edifice	28R 277972	3121876	350	Peg. Gab.	U. Mio.	10.8 ± 0.1 (3)
P3 suite							
Lag 3	Upper Old Edifice	28R 279777	3119425	350	Ta. M.	U. Mio.	9.1 ± 0.3 (1)
Lag 4	Upper Old Edifice	28R 279794	3119316	400	Ta. Sy.	U. Mio.	8.9 ± 0.1 (3)

S.-no.: sample numbers; Lag 1: La Gomera 1; P1, P2, P3: Intrusive complexes in the La Gomera Basal Complex (LG-BC) (Cendrero 1971; Démeny et al. 2010); Com.: Geological Complex; Elev.: Elevation; m.a.s.l.: metre above sea level; Lith.: Lithology; Pill.-bas.: pillow basalt; Subm. Trachy. Hyalocl.: submarine trachyte hyaloclastite; Am.-Gab.: Amphibole-Gabbro; Trach. (D): trachyte dike intruded into Lag 6, 7, 10; Am.-Pyrox.: Amphibole-Pyroxenite; Sy (D): syenite dike intruded in Lag 8; Peg. Gab.: pegmatitic gabbro; Ta. M.: Tamargada monzonite (plutonic ring complex); Ta. Sy.: Tamargada syenite (plutonic ring complex); Form. age: Formation ages taken from: (1) Cantagrel et al. (1984); (2): Herrera et al. (2008); (3) Casillas et al. (2022); L.-M.: Lower Miocene, M.-U. Mio: Middle–Upper Miocene; U. Mio: Upper Miocene; a.u.: age unknown. The transfer of radiometric ages into stratigraphic ages used the International Chronostratigraphic Chart version 2022/02 of the International Commission on Stratigraphy (Cohen et al. 2013)

of helium, out of an apatite grain) the chronometer is reset. Partial annealing or retention occurs when temperatures or required time did not fulfil the conditions for a total annealing/retention. For further interpretations, the following temperatures were used for *T*(c), and partial annealing (PAZ), or rather partial retention (PRZ) zones, respectively, for apatite and zircon, performed during this research:

- AHe: *T*(c): ~ 75 °C/1 Myr (Dodson 1973) and PRZ: between 70 °C/1 Myr and 40 °C/1 Myr (Wolf et al. 1996, 1998; Farley 1996, 2000; Stockli et al. 2000).
- AFT: *T*(c): 150 °C (high chlorine content) – 90 °C AFT (fluorine rich) and (PAZ): between 110 °C/10 Myr and 60 °C/10 Myr (Gleadow and Duddy 1981).
- ZHe: *T*(c): ~ 180 °C/1 Myr and PRZ: between 200 °C/1 Myr and 170 °C/1 Myr (Reiners et al. 2002, 2004).
- ZFT: *T*(c) between 330 °C/10 Myr (no metamictisation—a low degree of metamictisation) and 190 °C/10 Myr (high degree of metamictisation) (Garver and Kamp 2002; Garver 2003; Hurford 1986; Brix et al. 2002; Rahn et al. 2004; Reiners and Brandon 2006).

Numerical modelling of the time–temperature evolution

Numerical modelling of thermochronological data allows reconstructing the cooling history of crustal segments. A general law for numerical modelling of the *t–T* history of rocks is the increase in reliability with increasing amount of thermochronometers considered. The software code HeFTy® (v.1.9.3.) (Ketcham 2005, 2017; Ketcham et al. 2007a, b, 2009) was used to test potential time–temperature (*t–T*) paths against the thermochronological data set considering the published geological evolutions. Our aim was to test the hypotheses of Stillman (1999) that giant landslides have degenerate the first shield-stage volcanoes (initial Miocene Subaerial Volcanic Group) using our thermochronological data set. Relicts of this shield-stage volcanoes are the intrusive rocks of the North Basal Complex and the intrusive and sedimentary rocks of the West-Central Basal Complex. If the hypotheses are true, we expect to see a fast cooling event before the formation of the Stage C Miocene Subaerial Volcanic Complexes (Series I of Fúster et al. 1968). The software HeFTy® (v.1.9.3.) uses diffusion kinetics for the He-diffusion in apatite and zircon and annealing kinetics for the annealing of fission-tracks in apatite. The published geological evolution was transferred into *t–T*-constraints that are defined by geological events including a range of implied uncertainty (Table S1). For example: Sample Lag 1 was taken from a pillow basalt layer. Therefore, the initial start of the numerical modelling was at surface temperature. If, however, samples of intrusions were modelled the initial start temperature was a high as magma temperature provided by literature for such petrography. Furthermore, we try to provide less constrains as possible. The ZFT data are integrated as the second constrain and the *t–T* -box is kept very broad (Table S1). The third constrain is provided by the published geological evolution that provides evidence of near surface conditions for the intrusive rocks of the "Basal Complexes". The fourth constrain tested a possible thermal influence by volcanic rocks on the AFT- and AHe data. The software code runs *t–T* paths through the *t–T*-constrains areas to find possible solutions for a viable *t–T* history that fit the thermochronological input data. Statistical comparison (G.O.F.: goodness of fit) of the thermochronological data set generate by the possible *t–T* paths with the real thermochronological data set leads to the three categories: a best-fit *t–T* path (black line in the graphs), G: good *t–T* path, and A: acceptable *t–T* paths. The numerical models run until 1000 good *t–T* path have been found. Within the diagrams, the P describes the amount of *t–T* path runs to receive 1000 good *t–T* path. When possible, all available thermochronometers were combined and jointly modelled (Table S1; Table 9).

The thermochronological data sets used for the numerical modelling are:

- AHe: U-, Th-, and Sm concentration, radius of the single grains, uncorrected single grain ages, diffusion kinetics of Flowers et al. (2009).
- AFT: single grain ages, confined spontaneous fission-track length distribution (> 50 individual length) corrected for *c*-axis related angle (Donelick et al. 1999; Ketcham 2007a, b, 2009), etch pit size (D_{par}®), annealing kinetics of Ketcham et al. (2007a, b).
- ZHe: U-, Th-, and Sm concentration, radius of the single grains, uncorrected single grain ages, diffusion kinetics of Guenther et al. (2013).
- ZFT: as length data are not measured the central age was implemented as external *t–T* -constraints when necessary to improve thermal modelling

Thermochronological data

Fuerteventura Island

Zircon fission-track data

Four new samples revealed enough zircon grains for fission-track dating (Figs. 2, 4; Tables 3, 5). For better understanding, we also discuss and integrate the 6 already published ZFT ages of Wipf et al. (2010). All zircon grains of the magmatic rocks were etched with the same etching time and showed the same medium white colour, indicating a similar annealing temperature. Zircon fission-track ages of all

Table 5 Zircon and apatite fission-track data of samples from Fuerteventura Island (Table 1, Figs. 2, 3)

S.-no	Form. age (Ma)	U (std) (μg/g)	*n*	Sp. tracks		Ind. tracks		c^2 (%)	Cent. Age ± 1 s (Ma)	D_{par} (± std) (μm)
				ρ_s	N_s	ρ_i	N_i			
Northwest Basal Complex										
A1, A2, EM1 rock group; Montaña Blanca-Esquinzo sector										
Zr FU-38-09***	27.7 ± 1.2	*154.9 (99.2)*	*20*	*14.967*	*831*	*27.826*	*1.545*	*100*	*20.1 ± 1.3*	–
Ap FU-38-09***	27.7 ± 1.2	7.2 (12.2)	20	0.403	23	7.044	402	50	**14.2 ± 3.4**	2.2 ± 0.3
Ap FU-39-09***	Unknown	5.5 (4.9)	34	0.444	140	6.380	2.013	84	**16.4 ± 1.7**	1.8 ± 0.2
Zr FU-40-09***	27.3 ± 0.4	*86.8 (61.6)*	*8*	*9.492*	*171*	*17.262*	*311*	*100*	*20.5 ± 2.2*	–
Ap FU-40-09***	27.3 ± 0.4	2.3 (1.5)	29	0.173	37	2.906	622	76	**14.0 ± 2.5**	1.9 ± 0.5
Ap FU-41-09***	27.3 ± 0.5	2.4 (0.9)	28	0.181	24	2.843	378	96	**14.6 ± 3.2**	2.3 ± 0.3
Ap FU-42-09***	Unknown	2.4 (1.4)	20	0.151	10	2.771	184	97	**12.5 ± 4.1**	2.5 ± 0.3
Zr FU-43-09***	27.3 ± 0.6	*243.5 (219.1)*	*8*	*20.864*	*257*	*39.130*	*482*	*99*	*20.0 ± 1.8*	–
Ap FU-43-09***	27.3 ± 0.6	4.1 (6.6)	29	0.303	77	4.624	1.176	63	**14.9 ± 2.1**	2.1 ± 0.3
Ap FU-44-09***	27.3 ± 0.5	2.9 (2.0)	20	0.222	32	3.211	462	77	**15.6 ± 3.0**	1.9 ± 0.4
Ap FU-45-09***	28.3 ± 0.2	3.5 (3.5)	20	0.211	16	3.334	253	96	**14.2 ± 3.7**	1.9 ± 0.4
?A3, A4, EM3, EM4 rock group: Southern Northwest Basal Complex										
Ap FU-07-08**	unknown	5.5 (3.2)	32	0.427	93	5.694	1.239	100	**18.2 ± 2.1**	1.5 ± 0.1
Ap FU-09-08**	unknown	4.9 (0.9)	30	0.392	113	5.110	1.472	100	**18.6 ± 1.9**	1.8 ± 0.2
West-Central Basal Complex										
Sedimentary rock unit: North of Ajui										
Zr FU-02-07*	137–112	*192*	*13*	*51.758*	*234*	*72.550*	*328*	*8*	*58.6 ± 7.3*	–
Zr FU-06-07*	137–112	*137*	*5*	*27.953*	*62*	*45.987*	*102*	*92*	*50.0 ± 9.3*	–
Ap FU-06-07*	137–112	17	11	12.510	15	17.351	208	82	**14.5 ± 4.0**	–
Zr FU-08-07*	137–112	*228*	*6*	*58.913*	*128*	*82.846*	*180*	*34*	*51.7 ± 7.6*	–
Ap FU-08-07*	137–112	9	8	0.449	16	5.955	16	83	**15.1 ± 4.0**	–
Sheeted Dike Swarm unit: North of Ajui										
Ap Fu-03-07*	23–17	5	10	3.758	9	3.758	128	89	**14.1 ± 4.9**	–
Sheeted Dike Swarm unit: North of Montaña Sicasumbre										
Zr Fu-14-07*	23–17	*175*	*9*	*13.076*	*42*	*44.209*	*142*	*96*	*21.5 ± 4.3*	–
A1, A2, EM1 rock group: South of Ajui										
Ap FU-01-08**	26.2 ± 0.2	30.2 (8.5)	54	2.452	1115	32.831	14.927	42	**18.3 ± 0.9**	2.1 ± 0.1
Ap FU-02-08**	26.2 ± 0.2	5.7 (4.0)	35	0.358	87	5.528	1.345	100	**15.8 ± 1.8**	2.1 ± 0.3
?A3, A4, EM2, EM3 rock group: around Pajara?										
Ap FU-05-08**	Unknown	5.0 (2.1)	31	0.334	78	5.318	1.240	100	**15.3 ± 1.9**	1.6 ± 0.2
Ap FU-06-08**	Unknown	6.0 (3.4)	31	0.441	90	6.111	1.248	100	**17.5 ± 2.0**	1.5 ± 0.1
Unknown formation age West-Central Basal Complex										
Ap FU-03-08**	Unknown	3.4 (1.7)	103	0.058	30	3.405	1.776	98	**4.1 ± 0.8**	1.8 ± 0.4
Ap FU-04-08**	Unknown	3.9 (1.3)	217	0.047	21	4.288	1.912	100	**2.7 ± 0.6**	1.8 ± 0.2
East-Central Basal Complex										
A4 or EM3 rock group: Vega de Rio Palmas Ring Complex										
Zr FU-16-07*	18.7 ± 0.8	*31*	*8*	*1.895*	*19*	*10.573*	*106*	*77*	*15.6 ± 3.6*	–
Ap FU-16-07*	18.7 ± 0.8	23	18	1.303	36	21.933	606	99	**12.0 ± 2.1**	-
Zr FU-17-07*	18.4 ± 0.3	*606*	*6*	*65.501*	*236*	*240.078*	*865*	*98*	*19.3 ± 2.3*	–
Ap FU-17-07*	18.4 ± 0.3	6	19	0.451	52	6.499	750	100	**14.0 ± 2.1**	–
?A4, EM3, EM4 rock group: South of Betancuria?										
Ap Fu-01–10***	Unknown	4.9 (12.5)	20	0.503	97	5.471	1.055	92	**20.5 ± 2.4**	2.9 ± 0.5
Ap Fu-02–10***	Unknown	4.6 (3.3)	23	0.420	41	4.972	485	55	**19.1 ± 3.4**	2.2 ± 0.6
Ap Fu-03–10***	Unknown	3.6 (1.3)	14	0.320	28	3.853	337	94	**19.0 ± 3.9**	2.4 ± 0.4
Northern Volcanic Complex Suite I (NVC I): Tindaya trachytic dome										
Ap Fu-12-08**	18.7 ± 0.3	3.9 (1.3)	10	0.304	14	4.132	190	99	**17.8 ± 5.0**	1.5 ± 0.3

Table 5 (continued)

S.-no	Form. age (Ma)	U (std) (µg/g)	*n*	Sp. tracks		Ind. tracks		c^2 (%)	Cent. Age ± 1 s (Ma)	D_{par} (± std) (µm)
				ρ_s	N_s	ρ_i	N_i			
Central Volcanic Complex Suite I (CVC I)										
Zr FU-04–10***	20–21	*212.3 (123.1)*	*23*	*19.672*	*1676*	*36.979*	*3.143*	*100*	*19.6 ± 1.1*	-
Ap FU-04–10***	20–21	9.1 (7.5)	22	0.735	99	11.690	1.575	98	**14.5 ± 1.7**	1.6 ± 0.2

Zr zircon, *Ap* apatite, *U (std)* uranium concentration (standard deviation), *n* number of counted zircon and apatite grains, ρ_s density of spont. tracks (10^5 tr/cm^2), N_s number of spont. tracks, ρ_i density of induced tracks (10^5 tr/cm^2), N_i number of induced tracks, c^2 probability that single grain ages belong to the same population ($P(c^2) > 5\%$) (Galbraith 1981). –: not analysed. Zircon and apatite central ages are calculated with Trackkey 4.2 (Dunkl 2002)

*Data from Wipf et al. (2010)

**Data from M. Albinger: Apatite: ζ-value of 343.94 ± 12.56; Nd (CN5 dosimeter glass) = 15,279 tracks

***Data from S. Mansour: Zircon: ζ-value of 123.00 ± 6.09, Nd (CN1 dosimeter glass) = 16,413 tracks. Apatite: ζ-value of 330.60 ± 16.47; Nd (CN5 dosimeter glass) = 15,236 tracks. Series I–IV: Fúster et al. (1968), A1–A4: Balogh et al. (1999), EM1–EM4: Munoz et al. (2003)

Table 6 Zircon and apatite fission-track data of samples collected from La Gomera Island (Table 2, Fig. 3)

S.-no	Form. age (Ma)	U (± std) (µg/g)	*n*	Sp. tracks		Ind. tracks		c^2 (%)	Cent. Age ± 1σ (Ma)	D_{par} (± std) (µm)
				ρ_s	N_s	ρ_i	N_i			
Submarine volcanic rocks										
Ap Lag 1	11.5 ± 0.7	9.9 ± 10.0	27	0.651	202	14.373	4461	99	**10.7 ± 0–9**	2.9 ± 0.4
Ap Lag 2	10.98 ± 0.08	15.5 ± 5.8	14	0.742	65	22.360	1959	93	**8.9 ± 1.2**	3.0 ± 0.4
P1 suite										
Zr Lag 7	*10.6 ± 0.1*	*524.2 ± 387.9*	*22*	*21.800*	*996*	*92.127*	*4209*	*100*	*9.0 ± 0.5*	–
Zr Lag 10	*12.1 ± 0.1*	*418.6 ± 188.4*	*23*	*20.914*	*1415*	*82.430*	*5577*	*100*	*9.5 ± 0.5*	–
Zr Lag 11	*10.7 ± 0.1*	*277.2 ± 91.5*	*21*	*13.596*	*544*	*54.957*	*2199*	*100*	*9.2 ± 0.6*	–
Ap Lag 6	*10.6 ± 0.1*	14.9 ± 6.8	4	0.568	15	21.559	569	52	**6.9 ± 1.8**	2.3 ± 0.5
Ap Lag 9	10.4 ± 0.2	12.2 ± 4.7	24	0.286	60	15.270	3205	100	**4.8 ± 0.7**	1.8 ± 0.2
P2 suite										
Zr Lag 5	*10.6 ± 0.1*	*258.2 ± 116.2*	*25*	*11.716*	*624*	*52.385*	*2790*	*86*	*8.6 ± 0.5*	–
Ap Lag 5	10.6 ± 0.1	26.0 ± 16.1	5	0.930	24	32.314	834	98	**7.6 ± 1.6**	2.1 ± 0.5
Ap Lag 8	10.8 ± 0.1	6.9 ± 4.4	9	0.460	19	9.225	381	100	**12.9 ± 3.1**	2.3 ± 0.4
P3 suite										
Zr Lag 3	*9.1 ± 0.3*	*384.2 ± 184.4*	*18*	*18.269*	*893*	*74.673*	*3650*	*21*	*9.5 ± 0.6*	–
Ap Lag 3	9.1 ± 0.3	3.6 ± 0.9	34	0.120	36	4.963	1484	100	**6.5 ± 1.1**	2.1 ± 0.2
Zr Lag 4	*8.9 ± 0.1*	*230.8 ± 242.3*	*23*	*8.130*	*218*	*37.814*	*1014*	*100*	*8.3 ± 0.7*	–
Ap Lag 4	8.9 ± 0.1	4.9 ± 1.8	20	0.140	9	6598	424	95	**5.6 ± 1.9**	1.9 ± 0.2

U (std) uranium concentration and standard deviation in µg/g, *n* number of counted zircon and apatite grains, ρ_s density of spontaneous tracks (10^5 tr/cm^2), N_s number of spontaneous tracks, ρ_i density of induced tracks (10^5 tr/cm^2), N_i number of induced tracks, χ^2 probability that single grain ages belong to the same population ($P(\chi^2) > 5\%$) (Galbraith 1981). Zircon central ages are calculated with Trackkey 4.2 (Dunkl 2002) using a ζ-value of 120.00 ± 5.09 (S. Mansour). Nd (CN1 dosimeter glass) = 16,413 tracks. Apatite central ages are calculated with Trackkey 4.2 using a ζ-value of 330.60 ± 16.47 (S. Mansour). Nd (CN5 dosimeter glass) = 15,236 tracks. –: not analysed. From. age: Formation age see Table 2

samples range from 58.6 ± 7.3a to 15.6 ± 3.6 Ma with six samples in the range of 20.5 ± 2.2–19.3 ± 2.3 Ma. All samples passed the c^2-test indicating a homogeneous distribution with respect to 1σ-error of the single grain ages (Galbraith 1981). Nearly all ZFT ages are younger than the related intrusion or sedimentation age indicating a post-intrusion cooling history.

In the "Northwest Basal Complex", two carbonatites (#FU-38-09, #FU-40-09) and one pyroxenite sample (#FU-43-09) with the same intrusion age (27.6 ± 2.2 Ma), show the same ZFT age of av. 20.2 ± 1.8 Ma within error. In the "West-Central Basal Complex", zircon grains of three Lower Cretaceous sandstones (#FU-02-07, #FU-06-07, #FU-08-07) provide the oldest ZFT ages between 58.6 ± 7.3 Ma and 50.0 ± 9.3 Ma. Within error, the

Table 7 Confined fission-track length (CT), *c*-axes corrected CT (Lc), and D_{par} data of apatites revealed form various samples from Fuerteventura and La Gomera Island

Sample	CT *n*	CT mean (µm)	CT std (µm)	CT skew	Lc mean (µm)	Lc std (µm)	Lc skew	D_{par} *n*	D_{par} mean (µm)	D_{par} std (µm)	D_{par} skew
Fuerteventura Island											
Northwest Basal Complex											
A1, A2, EM1 rock group: Montaña Blanca-Esquinzo sector											
FU-39-09	101	14.0	1.5	− 1.101	14.9	1.4	− 1.677	505	2.2	0.3	0.851
FU-40-09	76	11.8	2.4	− 0.099	14.6	1.1	− 0.319	380	1.9	0.5	− 0.372
FU-41-09	61	12.8	2.2	− 0.602	14.1	1.5	− 0.528	305	2.3	0.3	− 0.602
FU-42-09	88	13.1	2.4	− 0.873	14.3	1.8	− 0.762	440	2.5	0.3	− 0.228
FU-43-09	106	13.3	2.0	− 1.301	14.3	1.6	− 1.287	530	2.1	0.2	− 0.238
FU-44-09	25	12.1	3.0	− 0.416	13.3	2.2	− 0.347	125	2.3	0.5	− 1.315
A3, A4, EM2, EM3 rock group: Southern Northwest Basal Complex											
FU-07-08	11	12.2	1.8	− 0.570	13.0	1.9	− 1.360	168	1.5	0.1	− 0.210
FU-09-08	5	14.1	2.7	− 0.750	14.9	1.8	0.380	160	1.8	0.2	− 2.000
West-Central Basal Complex											
A1, A2, EM1 rock group: South of Ajui											
FU-01-08	51	13.2	1.8	− 0.900	14.0	1.5	− 0.410	242	2.1	0.1	− 0.160
FU-02-08	5	11.2	2.4	0.200	12.2	2.0	0.420	107	2.1	0.3	− 0.780
A3, A4, EM2, EM3 rock group: around Pajara											
FU-05-08	9	12.7	3.0	− 0.250	13.3	3.0	− 0.510	185	1.6	0.2	3.170
FU-06-08	10	12.5	2.0	− 0.450	13.3	2.0	− 0.320	220	1.5	0.1	− 0.610
Unknown formation age West-Central Basal Complex											
FU-03-08	3	13.1	2.9	− 1.020	14.3	2.3	− 1.260	164	1.8	0.4	− 1.160
FU-04-08	1	13.9	–	–	13.9	–	–	122	1.8	0.2	− 0.310
La Gomera Island											
La Gomera Basal Complex											
Submarine volcanic suite											
Lag 1	141	14.4	1.4	− 1.507	15.2	1.2	− 1.665	705	2.9	0.4	− 0.437
P3 suite											
Lag 3	51	13.6	1.7	− 1.009	14.2	1.5	− 0.783	255	2.1	0.2	0.100
Lag 4	8	12.8	2.4	− 0.511	13.6	2.3	− 0.831	40	1.9	0.2	0.644

For further description, see Table 1. *CT n* number of measured confined tracks, *CT mean* mean confined track length, *std.* standard deviation, *skew.* skewness of distribution relative to the mean value, *Lc mean* mean track length after *c*-axis correction, D_{par} *n* number of measured etch pit, D_{par} *mean* mean etch pit size. Series I–IV: Fúster et al. (1968), A1–A4: Balogh et al. (1999), E1–E4: Munoz et al. (2003)

Table 8 Selection of the zircon and apatite (U–Th)/He data published by Wipf et al. (2019)

S.-no	F. age (Ma)	Ft	Weight (mg)	ccm ^{4}He (ccm STP)	Th/U	U (µg/g)	Th (µg/g)	Sm (µg/g)	eU (µg/g)	^{4}He (nmol/g)	Raw age ± 1σ (Ma)	Age ± 1σ (Ma)
Zircon												
West-Central Basal Complex												
Sedimentary rock unit: North of Ajui												
FU-02-07.1*	137–112	0.753	0.006	1.69E−09	0.58	135	78	n.a.	153	12.60	15.2 ± 1.2	20.2 ± 1.6
FU-02-07.2*		0.710	0.002	6.29E−10	0.70	133	93	n.a.	155	11.90	14.2 ± 1.1	19.9 ± 1.6
FU-02-07.3*		0.630	0.001	2.21E−10	0.40	130	52	n.a.	142	9.88	12.9 ± 1.0	20.5 ± 1.6
FU-02-07*												Av. 20.2 ± 1.6
FU-06-07.1*	137–112	0.749	0.006	5.69E−10	0.66	48	31	n.a.	55	4.28	14.5 ± 1.2	19.3 ± 1.5
FU-06-07.2*		0.766	0.004	5.49E−10	1.17	52	61	n.a.	66	5.78	16.2 ± 1.3	21.1 ± 1.7
FU-06-07.3*		0.844	0.021	5.24E−10	1.01	11	11	n.a.	14	1.10	15.2 ± 1.2	18.0 ± 1.4
FU-06-07*												Av. 18.0 ± 1.5
FU-08-07.2*	137–112	0.659	0.002	6.07E−10	0.35	247	86	n.a.	267	17.60	12.2 ± 1.0	19.5 ± 1.5
Sheeted Dike Swarm unit: North of Montaña Sicasumbre												
FU-14-07.1*	23–17	0.705	0.003	1.48E−09	0.54	370	201	n.a.	417	24.53	10.9 ± 0.9	15.5 ± 1.2
FU-14-07.2*		0.731	0.004	8.48E−10	0.59	147	86	n.a.	167	9.96	11.1 ± 0.9	15.1 ± 1.2
FU-14-07.3*		0.705	0.002	8.68E−10	0.50	270	134	n.a.	301	16.13	9.9 ± 0.8	14.1 ± 1.1
FU-14-07*												Av. 14.9 ± 1.2
East-Central Basal Complex												
A4, EM3 rock group: Vega de Rio Palmas Ring Complex												
FU-16-07.1*	16.05 ± 0.04–18.7 ± 0.8	0.752	0.005	2.16E−10	13.28	10	128	n.a.	40	2.16	10.0 ± 0.8	13.3 ± 1.1
FU-16-07.2*		0.665	0.002	1.99E−10	13.82	21	287	n.a.	88	4.36	9.1 ± 0.7	13.7 ± 1.1
FU-16-07*												Av. 13.5 ± 1.1
FU-17-07.1*	17.16 ± 0.40–18.4 ± 0.3	0.700	0.004	1.18E-09	1.82	187	339	n.a.	267	15.10	10.5 ± 0.8	15.0 ± 1.2
FU-17-07.2*		0.825	0.016	8.35E-09	2.12	240	509	n.a.	360	24.10	12.4 ± 1.0	15.0 ± 1.2
FU-17-07*												Av. 15.0 ± 1.2
Apatite												
West-Central Basal Complex												
Sedimentary rock unit: North of Ajui												
FU-02-07.1*	137–112	0.652	0.002	9.02E-11	0.81	51	41	2	61	4.02	12.3 ± 1.0	18.9 ± 1.5
FU-02-07.2*		0.560	0.001	1.40E-10	0.69	113	77	3	131	6.27	8.9 ± 0.7	15.8 ± 1.3
FU-02-07*												Av. 17.4 ± 1.4
FU-08-07/1*		0.572	0.001	3.09E-12	14.67	0	14	3	3	0.14	8.8 ± 0.5	15.4 ± 0.9
Sheeted Dike Swarm unit: North of Ajui												
FU-03-07.1*	23–17	0.586	0.001	1.85E-11	9.80	6	59	41	20	0.82	7.5 ± 0.6	12.8 ± 1.0
FU-03-07.2*		0.667	0.002	1.02E-11	8.86	3	24	34	9	0.45	9.6 ± 0.8	14.3 ± 1.1
FU-03-07*												Av. 13.6 ± 1.1

Table 8 (continued)

S.-no	F. age (Ma)	Ft	Weight (mg)	ccm ^{4}He (ccm STP)	Th/U	U (µg/g)	Th (µg/g)	Sm (µg/g)	eU (µg/g)	^{4}He (nmol/g)	Raw age ± 1σ (Ma)	Age ± 1σ (Ma)
East-Central Basal Complex												
A4, EM3 rock group: Vega de Rio Palmas Ring Complex												
FU-16-07.1*	16.05 ± 0.04–18.7 ± 0.8	0.665	0.001	4.34E-11	14.14	7	96	n.a.	30	1.33	8.3 ± 0.5	12.5 ± 0.8
FU-16-07.2*		0.713	0.003	3.48E-10	22.45	16	367	n.a.	102	5.00	9.0 ± 0.5	12.6 ± 0.8
FU-16-07*												Av. 12.6 ± 0.8
FU-17-07.3*	17.16 ± 0.40–18.4 ± 0.3	0.699	0.003	3.03E-11	5.16	5	25	n.a.	11	0.52	8.8 ± 0.5	12.5 ± 0.8
FU-17-07.3*		0.777	0.004	1.83E-10	4.75	19	92	n.a.	41	2.33	10.5 ± 0.7	13.5 ± 0.9
FU-17-07*												Av. 13.0 ± 0.9

The data were reexamined and for the first time are used for the numerical modelling of the time–temperature evolution. eU = [U] + 0.235 [Th] (concentration in µg/g)

F.-Age formation age, *n.a.* not analysed

individual ZFT ages are all equal and indicate a similar cooling history. A basic dike (#FU-14-07) occurring north of Montaña Sicasumbre in the sheeted dike swarm revealed an age of 21.5 ± 4.3 Ma, which is like the ZFT ages of the "Northwest Basal Complex". One syenite (#FU-16-07) and one gabbro (#FU-17-07) with an U–Pb zircon intrusion age of 16.05 ± 0.04 Ma–18.7 ± 0.8 Ma and 17.16 ± 0.40 Ma–18.4 ± 0.3 Ma, respectively, from the "Vega de Rio Palmas Ring Complex" ("East-Central Basal Complex") and one basaltic lava flow (#FU-04-10) of the CVC Series II (formation age of av. 20.8 ± 0.8 Ma) revealed the same ZFT age within error (15.6 ± 3.6 Ma; 19.3 ± 2.3 Ma; 19.6 ± 1.1 Ma, respectively). In comparison the U–Pb zircon intrusion ages of the "Vega de Rio Palmas Ring Complex" are within error the same as the zircon fission-track ages, therefore, the ZFT ages might indicate a fast cooling of the ring complex. Within error, the ZFT ages are like the ZFT ages of the intrusion samples from the "Northwest Basal Complex" and the "West-Central Basal Complex".

Formation ages The ZFT age (clear white zircon grains) of 19.6 ± 1.1 Ma of one lava flow within the "Miocene Volcanic Complex and Intrusions" (Series I) might represent the formation of the lava flow. The published assumed overlain thickness of the possible CVC Series does not reach a temperature of 300 °C for the analysed volcanic flow to reset the ZFT age. In addition, the flow did not show any indications for metamorphic or hydrothermal overprint.

Cooling ages The av. ZFT age of 53.4 ± 8.1 Ma of Lower Cretaceous sandstone samples are much younger than the age of sedimentation. We analysed clear white zircons, which represent closure temperatures of about 300 °C (Brix et al. 2002; Rahn et al. 2004). Therefore, those ages are interpreted as cooling ages. Similarly, the average age of 19.5 ± 2.4 Ma revealed from intrusions and one dike of the "Northwest Basal Complex", and the "West- and East-Central Basal Complex" are younger than the published intrusion ages and represent cooling ages.

Apatite fission-track data

21 new samples revealed enough apatite grains for fission-track dating (Figs. 2, 4; Tables 3, 5). For better understanding, we also discuss and integrate the 5 already published AFT ages of Wipf et al. (2010). AFT ages range from 20.5 ± 2.4 to 2.7 ± 0.6 Ma. All samples passed the c^2-test indicating a homogeneous distribution with respect to 1σ-error of the single grain ages (Galbraith 1981). One apatite fission-track ages is interpreted as a formation age. The other AFT ages are younger than the formation age of the

Table 9 Sample numbers, formation age, ZFT, ZHe, AFT, and AHe data used for numerical modelling

S.-no	Form. age (Ma)	ZFT (Ma)	ZHe (Ma)	AFT (Ma)	AHe (Ma)	Lc (μm)	D_{par} (μm)	Numerical modelling results		
								Modelled paths	Accept paths	Good paths
Fuerteventura Island										
Northwest Basal Complex										
A1, A2, A3 or EM1 rock group: Montaña Blanca-Esquinzo sector										
FU-39-09	27.6 ± 2.2	–	–	16.4 ± 1.7	n.a.	14.9 ± 1.4	2.2 ± 0.3	104,249	5806	1000
FU-40-09	27.2 ± 2.2	20.5 ± 2.2	n.a.	14.0 ± 2.5	n.a.	14.6 ± 1.9	1.9 ± 0.5	133,708	6777	1000
FU-41-09	27.3 ± 0.5	–	–	14.6 ± 3.2	n.a.	14.1 ± 1.8	2.3 ± 0.3	29,618	2993	1000
FU-42-09	27.3 ± 2.2	–	–	12.5 ± 4.1	n.a.	14.3 ± 1.8	2.5 ± 0.3	1.06 E + 06	31,882	1000
FU-43-09	27.3 ± 0.6	20.0 ± 1.8	n.a.	14.9 ± 2.1	n.a.	14.3 ± 1.6	2.1 ± 0.5	1.04 E + 06	23,663	1000
West-Central Basal Complex										
Sedimentary rock unit: North of Ajui										
FU-02-07*	137–112	58.6 ± 7.3	20.2 ± 1.6 19.9 ± 1.6 20.5 ± 1.6	–	18.9 ± 1.5 15.8 ± 1.3			2.88 E + 06	25,237	1000
FU-06-07*	137–112	50.0 ± 9.3	19.3 ± 1.5 21.1 ± 1.7 18.0 ± 1.4	14.5 ± 4.0	n.a.			23,503	1711	1000
FU-08-07*	137–112	51.7 ± 7.6	18.5 ± 1.5	15.1 ± 4.0	15.4 ± 0.9			1.07 E + 06	3976	1000
Sheeted Dike Swarm unit: North of Ajui										
FU-03-07*	23–17	–	–	14.1 ± 4.9	12.8 ± 1.0 14.3 ± 1.1			161,460	2915	1000
Sheeted Dike Swarm unit: North of Montaña Sicasumbre										
FU-14-07*	23–17	21.5 ± 4.3	15.5 ± 1.2 15.1 ± 1.2 14.1 ± 1.1	–	–			162,428	8544	1000
A1, A2, A3 or EM1 rock group: South of Ajui										
FU-01-08	26.2 ± 0.2	–	–	18.3 ± 0.9	n.a.	14.0 ± 1.5	2.1 ± 0.1	228,767	8726	1000
East-Central Basal Complex										
A4 or EM3 rock group: Vega de Rio Palmas Ring complex										
FU-16-07*	18.7 ± 0.6	15.6 ± 3.6	13.1 ± 1.1 13.7 ± 1.1	12.0 ± 2.1	12.5 ± 0.8 12.6 ± 0.8 12.5 ± 0.8			386,946	3272	1000
FU-17-07*	18.4 ± 0.3	19.3 ± 2.3	15.0 ± 1.2 15.0 ± 1.2	14.0 ± 2.1	15.7 ± 1.0 16.8 ± 1.1 13.5 ± 0.9			173,892	3875	1000

Table 9 (continued)

S.-no	Form. age (Ma)	ZFT (Ma)	ZHe (Ma)	AFT (Ma)	AHe (Ma)	Lc (µm)	D_{par} (µm)	Numerical modelling results		
								Modelled paths	Accept paths	Good paths
La Gomera Island										
La Gomera Basal Complex										
Submarine volcanic suite										
Lag 1	11.5 ± 0.7	–	–	10.7 ± 0.9	n.a.	15.2 ± 1.2	2.9 ± 0.4	379,540	6779	1000
P3 suite										
Lag 3	8.9 ± 0.1	10.3 ± 0.5	n.a.	6.5 ± 1.1	n.a.	14.2 ± 1.5	2.1 ± 0.2	28,175	4405	1000

Lc > 50 length measured, D_{par} > 240 length, *n.a.* not analysed, – no grains

Numerical modelling path: modelled path to achieve 1000 good path. Initial mean track length: 16.3 µm from D_{par}; track length reduction standard: 0.893; kinetic parameter: D_{par}; present day temperature 15 °C ± 5 °C; FT-annealing model: Ketchem et al. (2007a), etching model Ketchem et al. (2007b); *c*-axis projection; segment parameters are monotonic consistent, episodic; maximum cooling rate: 10 °C/Ma; He-diffusion model for apatite: Flowers et al. (2009); He-diffusion model for zircon: Guenther et al. (2013)

magmatic and sedimentary samples. Therefore, we interpreted those ages as cooling ages.

Formation ages The Tindaya trachyte (#FU-12-08) has a formation age of 18.7 ± 0.3 Ma, and an AFT age of 17.8 ± 5.0 Ma. Within error, the AFT age is the same as the formation age. Therefore, the AFT age might indicate a fast cooling of the Tindaya trachyte and no heating above 60 °C afterwards.

Cooling ages Even that the AFT ages have a large range, three cluster can be seen including the error in the data:

Cluster I: 20.5 ± 2.4 Ma–17.5 ± 2.0 Ma; av. 18.7 ± 2.4 Ma.

One layered gabbro (#FU-07-08) and one coarse-grained gabbro (#FU-09-08) form the southern side of the "Northwest Basal Complex" show AFT ages of 18.2 ± 2.1 Ma and 18.6 ± 1.9 Ma, respectively. These ages are within error like the AFT ages revealed for a carbonatite (#FU-01-08: 18.3 ± 0.9 Ma) and basic dike (#FU-06-08: 17.5 ± 2.0 Ma) of the "West-Central Basal Complex", a trachyte (#FU-02-10: 19.1 ± 3.4 Ma), and two coarse-grained syenite (#FU-01-10: 20.5 ± 2.4 Ma, #FU-03-10: 19.0 ± 3.9 Ma) from the "East-Central Basal Complex" (Betancuria Complex), and the formation age of the Tindaya trachyte.

Cluster II: 16.4 ± 1.7 Ma–12.5 ± 4.1 Ma; av. 14.5 ± 2.9 Ma.

Eight AFT ages of carbonatites (#FU-38-09: 14.2 ± 3.4 Ma; #FU-40-09: 14.0 ± 2.5 Ma), pyroxenites (#FU-39-09: 16.4 ± 1.7 Ma; #FU-42-09: 12.5 ± 4.1 Ma), Ijolites (#FU-41-09: 14.6 ± 3.1 Ma; #FU-44-09: 15.6 ± 3.0 Ma), and syenite dikes (#FU-43-09: 14.9 ± 2.1 Ma; #FU-45-09: 14.2 ± 3.7 Ma) of the "Northwest Basal Complex" are within error the same. Similarly, the AFT ages of two syenites (#FU-02-08: 15.8 ± 1.8 Ma; #FU-05-08: 15.3 ± 1.9 Ma), a basic dike (#FU-03-07: 14.1 ± 4.9 Ma), and two Lower Cretaceous sandstone (#FU-06-07: 14.5 ± 4.0 Ma; #FU-08-07: 15.1 ± 4.0 Ma) of the "West-Central Basal Complex", AFT age of a syenite (#FU-16-07: 12.0 ± 2.1 Ma) and a gabbro (#FU-17-07: 14.0 ± 2.1 Ma) of the "East-Central Basal Complex" and one basaltic flow (#FU-04-10: 145 ± 1.7 Ma) of the CVC II suite are within this age cluster.

Cluster III: 4.7 ± 0.8 Ma–2.7 ± 0.6

Two NE–SW-trending fine-grained trachytic dikes of unknown formation age that cut Lower Cretaceous sedimentary rocks in the "West-Central Basal Complex" revealed AFT ages of 2.7 ± 0.6 Ma and 4.7 ± 0.8 Ma. These dikes are located close (tenth of metre) to a large Pliocene basaltic flow of the Series II. They might have been thermally influenced by the basaltic flow. Therefore, it cannot be excluded that the age might represent a reheating and, thereafter, fast cooling caused by the Pliocene basaltic flow.

The average etch pit size, called D_{par}, range from 2.9 ± 0.5 to 1.5 ± 0.1 µm. Apatite grains of one coarse-grained syenite show the larges etch-pits. Within error, all apatites of the carbonatites and syenites are characterised by D_{par} values above 2.0 µm. No relation between AFT ages and D_{par} has been encountered. Generally, AFT ages do not show any trends when compared to their elevation or spatial distribution.

Only six samples, five of the "Northwest Basal Complex" and one of the "West-Central Basal Complex", revealed more than 50 length measurements of confined fission-track (CT) to perform the numerical modelling of the *t–T* evolution (CT's: 106–51; Table 7). Eight samples provided length measurements between 1 and 23 confined fission-tracks. The mean confined fission-track length values range from 11.2 ± 2.4 to 14.0 ± 1.5 µm. The skewness of 12 CT-data is negative. One showed a positive skewness. The *c*-axes correction of the confined track lengths led to a corrected confined fission-track length (Lc) distribution between 12.1 ± 2.0 and 14.9 ± 1.8 µm. The long Lc distribution indicates a fast cooling history for the analysed samples. The etch pit size D_{par} of each apatite grain was determined for all samples used for length measurement. The mean D_{par} values range from 2.5 ± 0.3 to 1.5 ± 0.1 µm indicating a domination of fluorine-rich apatite grains.

Re-interpretation of published zircon (ZHe) and apatite (AHe) (U–Th)/He data

Three Lower Cretaceous sandstones and one lower Miocene magmatic dike of the "West-Central Basal complex" and one syenite and one gabbro of the "East-Central Basal Complex" samples revealed well-shaped zircon (3–1) and apatite grains (3 or 2) for (U–Th)/He dating (Table 8; Figs. 2, 4). The He age variation of single zircon grains within one sample are within error. No correlation between the eU-value and the determined ZHe and AHe ages exists. The ZHe single grain ages vary from 21.1 ± 1.7 to 13.3 ± 1.1 Ma and are younger than the formation age indicating cooling ages. The zircon (U–Th)/He ages of the gabbro (#FU-16-07*) and syenite (#FU-17-07*) are in average younger (av. 14.3 ± 1.2 Ma) than those of the sandstones (#FU-02-07*, #FU-06-07*, #FU-08-07*: av. 19.5 ± 1.6 Ma). Considering the diffusion behaviour of He in zircon grains a temperature below 185 °C was reached much earlier for the "West-Central Basal complex" than for the "East-Central Basal Complex". One basaltic dike (#FU-14-07*) of the sheeted dike complex ("West-Central Basal Complex") revealed an average ZHe cooling age of 14.9 ± 1.2 Ma, which is within error the same as the ZHe cooling age of the "East-Central Basal Complex".

In general, the AHe single grain ages vary from 18.9 ± 1.5 to 12.5 ± 0.8 Ma. Two sandstone samples (#FU-02-07*, #FU-08-07*) and the dike sample (#FU-14-07*) of the "West-Central Basal complex" revealed AHe single grain ages between 18.9 ± 1.5 and 12.8 ± 1.0 Ma. The two samples of the "East-Central Basal Complex" (#FU-16-07*, #FU-17-07*) provide AHe single grain ages between 13.5 ± 0.9 Ma and 12.5 ± 0.8 Ma. All AHe ages are cooling ages.

Time–temperature (*t–T*) numerical modelling

The numerical modelling of the *t–T* path for the samples with either more than 50 confined fission-track length or (U–Th)/He data revealed an area of acceptable (green colour), good (orange colour), and one best-fit *t–T* path (black). In general, the goodness of fit (G.O.F.) is more than 0.87. The best constrained *t–T* path would have a G.O.F. of 1.0. In some cases, such as the AHe data of the Lower Cretaceous sandstone (#FU-02-07*), the G.O.F. is lower in value and, therefore, part of the *t–T* path is less well constrained. The reasons for the *t–T* boxes are described in "Numerical modelling of the time–temperature evolution".

Northwest Basal Complex Samples of two pyroxenite (#FU-39-09, #FU-42-09), one Ijolite (#FU-41-09), one carbonatite (#FU-40-09), and one syenite (#FU-43-09) of the "Northwest Basal Complex" revealed enough confined fission-track length to perform numerical modelling of the *t–T* evolution (Tables 3, 5, 9, S1; Fig. 5). The average Oligocene formation age of the intrusions is 27.3 ± 0.5 Ma (Casillas et al. 2022). The five samples are located within an area of ~ 4 km^2 (Fig. 2).

A moderate cooling from ~ 500 to 280 °C within 7 Myr since the formation (27.3 ± 0.6 Ma) is followed by a decrease in *T* reaching low temperatures (40–20 °C) at ~ 19 Ma in less than 1 Myr. In all five cases, the best-fit *t–T* path is nearly vertical. Reheating is excepted by the thermochronological data and lead to a maximum *T* of ~ 80 °C at ~ 14 Ma for a short time. The amount of reheating is different in the samples analysed. Thereafter, the temperature decreases to recent surface temperature.

Summarising the possible *t–T* evolution of the best-fit path, the *t–T* evolution is characterised by four major pattern:

- ~ 27 Ma to ~ 19 Ma: moderate cooling from ~ 500 to ~ 280 °C.
- ~ 19 Ma: rapid cooling from 280 to ~ 40 °C–20 °C.
- ~ 19 Ma to ~ 14 Ma reheating from ~ 20 to ~ 80 °C.
- ~ 14 Ma–recent: slow cooling from ~ 80 to 20 °C.

West-Central Basal Complex Three Cretaceous sandstones (#FU-02-07*, #FU-06-07*, #FU-08-07*, Form. age: 137–112 Ma), and two Upper Oligocene basic dikes (#FU-03-07*, #FU-14-07*, Form. age: 24–17 Ma) of the sheeted dike complex revealed zircon and/or apatite (U–Th)/He single grain ages that have been used to remodel the *t–T* evolution

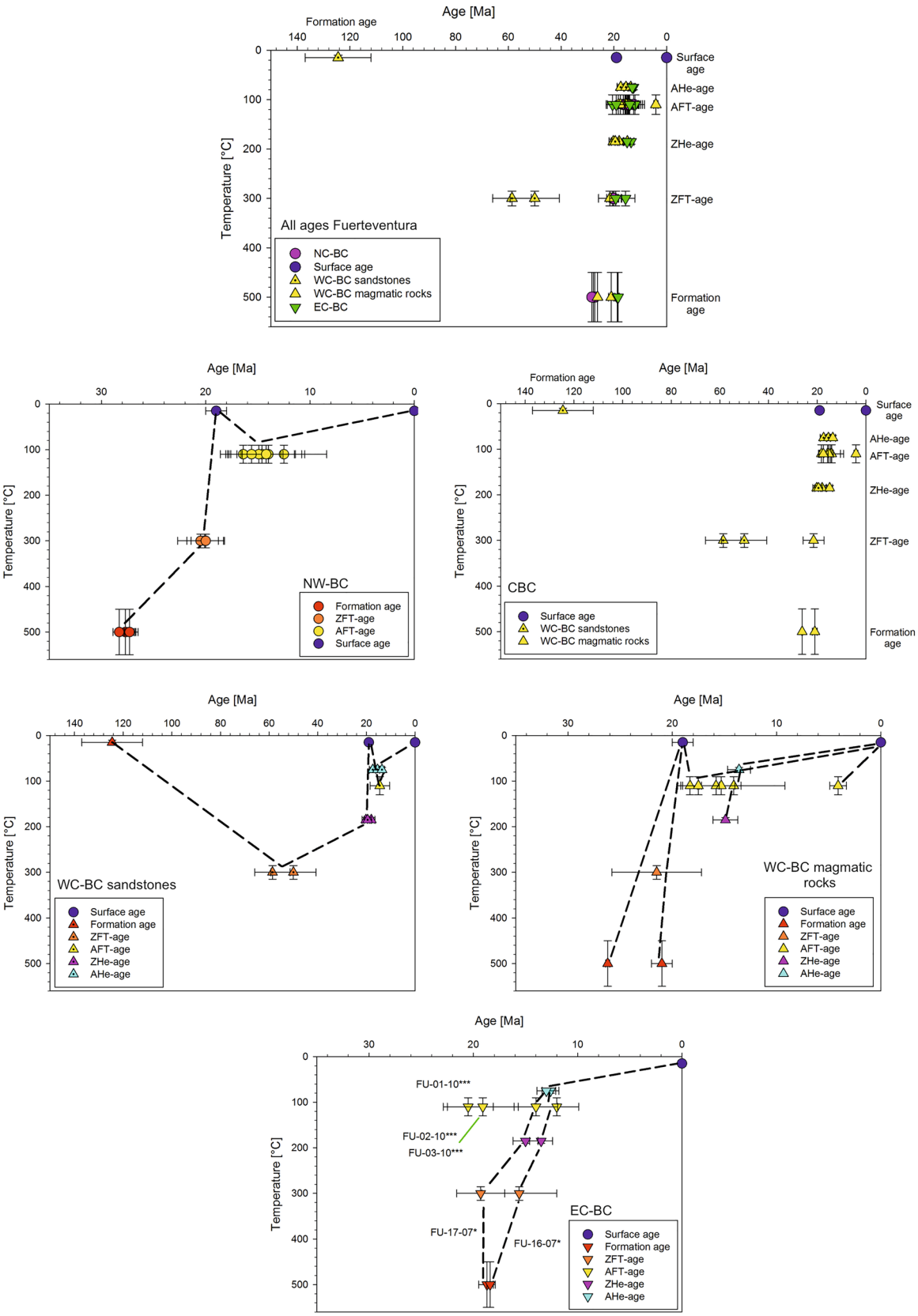
Age [Ma]
Formation age
Surface age
AHe-age
AFT-age
ZHe-age
ZFT-age
Formation age
Temperature [°C]
All ages Fuerteventura
NC-BC
Surface age
WC-BC sandstones
WC-BC magmatic rocks
EC-BC
NW-BC
Formation age
ZFT-age
AFT-age
Surface age
CBC
Surface age
WC-BC sandstones
WC-BC magmatic rocks
WC-BC sandstones
Surface age
Formation age
ZFT-age
AFT-age
ZHe-age
AHe-age
WC-BC magmatic rocks
Surface age
Formation age
ZFT-age
AFT-age
ZHe-age
AHe-age
FU-01-10***
FU-02-10***
FU-03-10***
FU-17-07*
FU-16-07*
EC-BC
Surface age
Formation age
ZFT-age
AFT-age
ZHe-age
AHe-age

◂**Fig. 4** Formation ages and thermochronological ages of the four areas in Fuerteventura. Temperature according to the known final diffusion and annealing temperature at a cooling rate of 10 °C/Ma. As part of the "Basal Complexes" are overlain by subaerial volcanic rocks younger than 20 Ma, intrusive and sediment rocks of the "Basal Complex" must have been at the surface before the subaerial volcanic rocks were deposited. If not otherwise mentioned, the dashed lines represent possible heating and cooling path between the thermochronological ages of the area. *NW-BC* Northwest Basal Complex, *CBC* Central Basal Complex, *WC-BC* West-Central Basal Complex, *EC-BC* East-Central Basal Complex. The age of the Garajonay landslide is taken from Paris et al. (2005)

(Tables 3, 5, 8; Figs. 6, 7). One Upper Oligocene carbonatite dike (#FU-01-08, formation age: 26.2 ± 0.2 Ma) provided enough confined apatite fission-track length to perform the numerical modelling of the *t–T* evolution.

Sandstones and basaltic dikes The *t–T* evolution of sandstone #FU-02-07* and #FU-08-07* are well constrained as up to three zircon grains and up to two apatite grains have been used for the numerical modelling. The third sandstone (#FU-06-07*) is less constrained. The three sandstones revealed a similar *t–T* evolution from formation to the Lower Miocene (20 Ma). A Gradual increase of temperature from surface temperature at sedimentation age (open box between 137 and 112 Ma) can be observed reaching ~ 300 °C at about 55 Ma, which is coherent with the described metamorphic grade by Steiner et al. (1998), and the ZFT ages. A moderate decrease in temperature reached ~ 250 °C at 20 Ma. Thereafter, the *t–T* path indicates that the sandstones cooled rapidly to a temperature between 40 and 20 °C at ~ 20 Ma. The two sandstones #FU-02-07* and #FU-08-07* which are located close to each other are kept at surface temperature until today. The same constrains for the numerical modelling of the sandstone #FU-06-07* indicate a *t–T* path that is quite different. This sandstone might have been reheated to ~ 80 °C at ~ 14 Ma and cooled, thereafter, to recent surface temperatures.

Basic dikes One basic dike (#FU-03-07*) is crossing the sandstones in N–S direction. The second basic dike (#FU-14-07*) is attributed to the sheeted dike complex further to the South of the Island. For both basic dikes the numerical modelling exhibits a similar *t-T* evolution showing fast cooling from ~ 500 to ~ 50 °C (#FU-03-07*) and 75 °C (#FU-14-07*), respectively, between their formation age (24–20 Ma) and ~ 20 Ma. An increase in T occurs during the Miocene and reached temperature between ~ 75 °C (#FU-03-07*) and ~ 115 °C (#FU-14-07*) at ~ 14 Ma. Cooling leads to surface temperature at ~ 10 Ma (#FU-03-07*) recent time (#FU-14-07*).

Carbonatite dike (#FU-01-08, Form. age: 26.2 ± 0.2 Ma) The *t–T* path indicates a fast cooling from 450 to 50 °C at ~ 22 Ma. Between ~ 22 and ~ 18 Ma, the dike cooled to surface temperature. The following increase in temperature reached a maximum of ~ 80 °C at about ~ 14 Ma. Decrease in temperature reached surface temperature at recent time again.

Summarising the *t–T* evolution of the "West-Central Basal Complex" leads to the following:

- at ~ 55 Ma the sandstones reached a maximum temperature of ~ 300 °C °C in average and kept the temperature until ~ 21 Ma.
- at ~ 21 Ma rapid cooling to near surface temperature happened to the sandstones and the basic dikes of the sheeted dike swarm complex.
- at ~ 14 Ma reaching a new individual maximum T of ~ 80 to ~ 115 °C.
- at ~ 14 Ma rapid decrease in T to surface temperature of nearly all analysed samples (cooling by 60–95 °C). The surface temperature is kept until recent.

East-Central Basal Complex One syenite (#FU-16-07) and one gabbro (#FU-17-07) of the Vega de Rio Palmas Ring complex revealed zircon and/or apatite (U–Th)/He single grain ages that have been used to model the *t–T* evolution (Tables 3, 5, 8; Fig. 8). The *t–T* evolution of syenite #FU-16-07* is well constrained as two zircon grains and three apatite grains have been used for the numerical modelling. In addition, the regional geological evolution indicated that the intrusive rocks were covered with volcanic rocks at about 15 Ma.

A moderate cooling ~ 550 °C to ~ 250 °C occurred between ~ 18 and ~ 16 Ma. Thereafter, the temperature dropped nearly instantaneously at ~ 15 Ma to ~ 30 °C. Temperature increase reached ~ 80 °C at ~ 14 Ma and is followed by a rapid decrease of *T* to surface temperature. The surface temperature was kept until recent time.

Summarising the *t–T* evolution four major pattern is seen:

- moderate cooling ~ 550 to ~ 250 °C occurred between ~ 18 Ma and ~ 15 Ma.
- rapid cooling at ~ 15 Ma from intrusion temperature to near surface temperature.
- reheating to a maximum *T* of 80 °C at ~ 14 Ma.
- rapid decrease of *T* to surface temperature at ~ 14 Ma. Surface *T* was kept until recent.

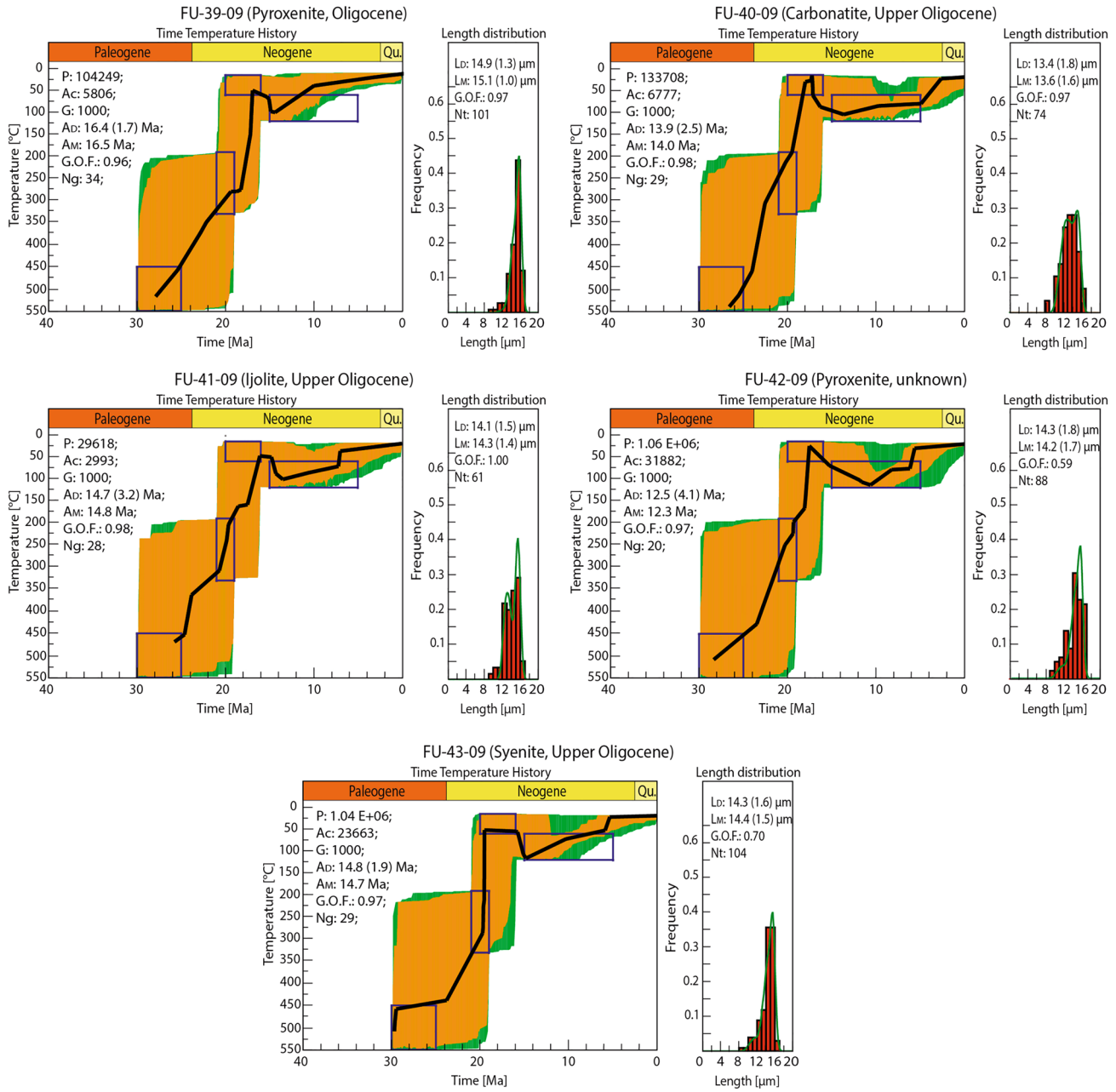

Fig. 5 Thermal history models of the samples from the "Northwest Basal Complex" modelled using the software code HeFTy (Ketcham et al. 2007a, b, 2009). The left window displays the *t–T* paths, the right column displays the *c*-axes corrected confined fission-track lengths distribution overlain by a calculated probability density function for the best-fit *t–T* solution. All constrains are provided in Table S1. Resulting *t–T* curves show three different path envelopes; green path envelope: acceptable fit (all *t–T* paths with a merit function value of at least 0.05), orange path envelope: good fit (all *t–T* paths with a merit function value of at least 0.5), and black line: best-fit path of all accepted and good paths (Ketcham et al. 1999, Ketcham et al. 2007a, b, 2009). *P* amount of *t–T* path runs necessary to receive 1000 good *t–T* path, *Ac* acceptable fit models, *G* good fit models, A_D determined FT age with 1−σ error, A_M modelled FT age, L_D determined central *c*-axes corrected confined fission-track length with 1−σ error, L_M modelled confined fission-track length with 1−σ error, *G.O.F.* goodness of fit, *Ng* number of single grains, *Nt* number of single confined fission-tracks

La Gomera Island

Zircon fission-track (ZFT) data

Six samples from the suite P1, P2, and P3 of the "La Gomera Basal Complex" revealed enough zircon grains for fission-track dating (Tables 4, 6; Figs. 3, 9). ZFT central ages range between 9.5 ± 0.6 Ma and 8.3 ± 0.7 Ma (Figs. 3, 9; Table 6). All samples passed the c^2-test indicating a homogeneous distribution with respect to 1σ-error of the single grain ages (Galbraith 1981). With the exceptions of #Lag 3 (9.5 ± 0.6 Ma) and #Lag 4 (8.3 ± 0.7 Ma) sample (Tamargada monzonite and syenite) the ZFT ages are slightly younger than the related extrusion or intrusion age. The samples #Lag 5 (8.6 ± 0.5 Ma), #Lag 7 (9.0 ± 0.5 Ma), #Lag 10 (9.5 ± 0.5 Ma), and #Lag 11 (9.2 ± 0.6 Ma) are located within a narrow area in the NW of the Island. The ZFT cooling ages are within error the same with an average cooling age of 9.1 ± 0.5 Ma, which is similar to the proposed intrusion age of the Tamargada syenite (9.1 ± 0.3 Ma). The Tamargada monzonite sample (#Lag 3) revealed a ZFT age of 9.5 ± 0.6 Ma, which correlates with the proposed intrusion age of 8.9 ± 0.1 Ma within error. The Tamargada syenite sample (#Lag 4) revealed an age of 8.3 ± 0.7 Ma, which also shows the same age within error as the proposed intrusion age of 9.1 ± 0.3 Ma. Within error, both ZFT ages correlate with the proposed average formation age of 9.0 ± 0.2 Ma of the Tamargada complex. Both ages indicate a fast cooling from magma intrusion temperature to the zircon fission-track annealing temperature. As the zircon grains were clear white with a long etching time, we assume that the ZFT age represent a total annealing temperature of about 300 °C.

Summarising the ZFT ages and considering the error only two age groups can be recognised:

- av. 8.9 ± 0.7 Ma: ZFT formation age of the Tamargada monzonite and syenite and fast cooling to below 300 °C.
- av. 9.1 ± 0.5 Ma: ZFT cooling ages of samples (#Lag 5, 7, 10, 11) located close to each other. Extreme interesting is that within error the ZFT age is the same as the intrusion age of the Tamargada ring complex.

Apatite fission-track (AFT) data

Eight samples (submarine volcanic rocks, P1, P2, P3 suites, a trachyte breccia) of the "La Gomera Basal Complex" revealed enough apatite grains for fission-track dating (Tables 4, 6; Figs. 3, 9). The AFT ages range between 12.9 ± 3.1 Ma and 4.8 ± 0.7 Ma. All samples passed the c^2-test indicating a homogenic population in each sample set. Except for #Lag 8 all AFT ages are younger than the related extrusion or intrusion age indicating a post-extrusion and intrusion cooling history. The oldest AFT age (12.9 ± 3.1 Ma) of a pegmatitic gabbro (#Lag 8, P2 suite) is within error the same as the proposed intrusion age (10.8 ± 0.1 Ma). Considering the D_{par} of 2.3 ± 0.4 µm a very fast cooling to a temperature of 110 °C or even below might have occurred. The AFT age (10.7 ± 0.9 Ma) of the pillow basalt (#Lag 1, submarine volcanic rocks) correlates with the proposed extrusion age (11.5 ± 0.7 Ma) within error. The AFT ages (7.6 ± 1.6 Ma) of a syenite dike (#Lag 5, P2 suite,) and the AFT age (6.9 ± 1.8 Ma) of an amphibole gabbro (#Lag 6, P3 suite) with the same intrusion age (10.6 ± 0.1 Ma) are of the same age. Similarly, ages are revealed by #Lag 3 (6.5 ± 1.1 Ma; Tamargada monzonite, P3 suite), and #Lag 4 (5.6 ± 1.9 Ma; Tamargada syenite, P3 suite). Therefore, an average AFT age of 6.7 ± 1.6 Ma is calculated using the AFT ages of #Lag 3, 4, 5, and 6. A submarine hyaloclastite (#Lag 2) of 11.0 ± 0.2 Ma showed an AFT age of 8.9 ± 1.2 Ma. This age also correlates with the average age 6.7 ± 1.6 Ma of #Lag 3, 4, 5, and 6 within error. A trachyte dike (#Lag 9) with a formation age of 10.4 ± 0.2 Ma provided the youngest AFT age of 4.8 ± 0.7 Ma.

The average D_{par} size, range from 3.0 ± 0.4 to 1.8 ± 0.2 µm. Apatite grains of the trachyte breccia and the basic pillow lava show the larges etch-pits. Within error, all apatite grains of the amphibole gabbro, the syenite, the pegmatitic gabbro, and Tamargada monzonite are characterised by D_{par} values above 2.0 µm. No relation between AFT ages and D_{par} has been encountered. The elevation of the samples range between 430 m.a.s.l. and 3 m.a.s.l. Comparing all ages with the elevation did not provide any indication for an elevation dependency of the AFT ages.

Only two samples (#Lag 1, #Lag 3) revealed enough confined spontaneous fission-track length (CT, > 50) and etch pit size (D_{par}®) data to perform numerical modelling of the *t*–*T* evolution showing D_{par}® values between 1.9 ± 0.2 and 2.9 ± 0.4 µm (average: 1.2 µm). Mean track lengths vary between 13.6 ± 1.7 µm (#Lag 3) and 14.4 ± 1.4 µm (#Lag 1). Lag 4 only revealed eight confined fission-tracks with an average fission-track length distribution of 12.8 ± 2.4 µm. In general, the skewness of the three CT-data is negative. The *c*-axes correction of the confined track lengths (Lc) led to a length distribution between 13.6 ± 2.3 and 15.2 ± 1.2 µm. Generally, Lc distributions showing longer lengths indicate a fast exhumation history. Even that these three samples provide a positive correlation between the average D_{par}-value and the AFT central Age, including the other samples no correlation is in the data. According to Burtner et al. (1994), Donelick et al. (2005) and Barbarand et al. (2003), the large D_{par} indicate Cl-rich apatite grains and short D_{par} F-rich apatite grains.

Summarising the AFT ages and considering the error three age groups can be recognised:

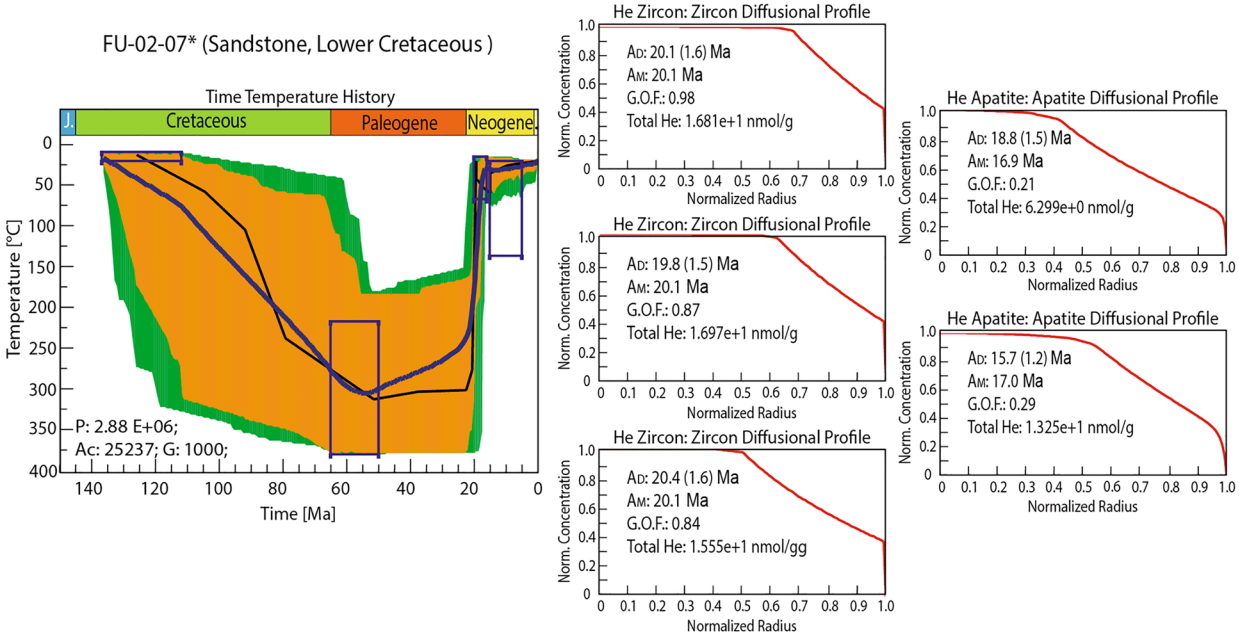
FU-02-07* (Sandstone, Lower Cretaceous)
Time Temperature History
J.
Cretaceous
Paleogene
Neogene
Temperature [°C]
Time [Ma]
P: 2.88 E+06;
Ac: 25237; G: 1000;
He Zircon: Zircon Diffusional Profile
AD: 20.1 (1.6) Ma
AM: 20.1 Ma
G.O.F.: 0.98
Total He: 1.681e+1 nmol/g
He Apatite: Apatite Diffusional Profile
AD: 18.8 (1.5) Ma
AM: 16.9 Ma
G.O.F.: 0.21
Total He: 6.299e+0 nmol/g
He Zircon: Zircon Diffusional Profile
AD: 19.8 (1.5) Ma
AM: 20.1 Ma
G.O.F.: 0.87
Total He: 1.697e+1 nmol/g
He Apatite: Apatite Diffusional Profile
AD: 15.7 (1.2) Ma
AM: 17.0 Ma
G.O.F.: 0.29
Total He: 1.325e+1 nmol/g
He Zircon: Zircon Diffusional Profile
AD: 20.4 (1.6) Ma
AM: 20.1 Ma
G.O.F.: 0.84
Total He: 1.555e+1 nmol/gg
Norm. Concentration
Normalized Radius

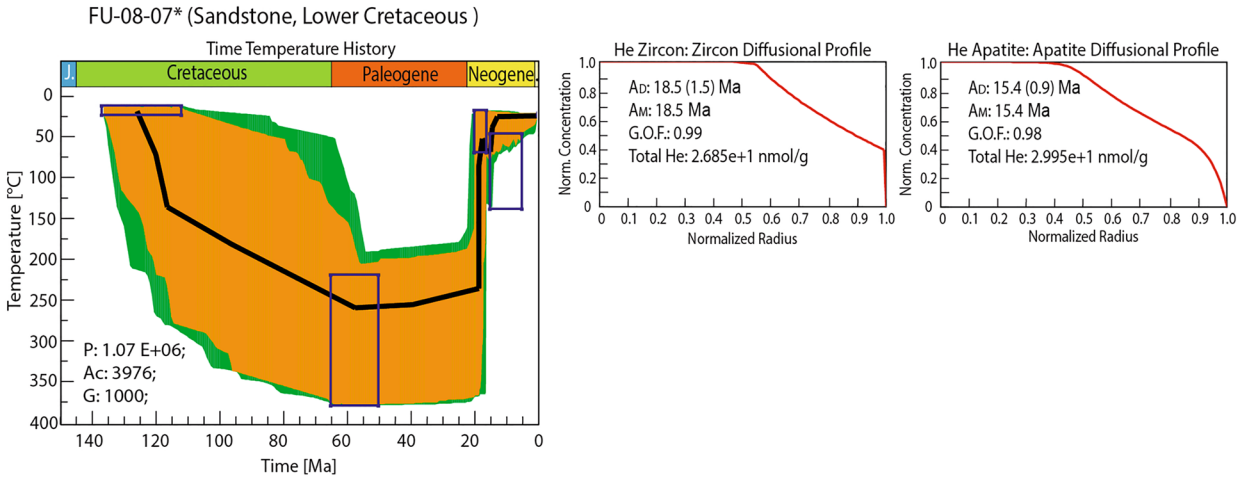
FU-08-07* (Sandstone, Lower Cretaceous)
Time Temperature History
J.
Cretaceous
Paleogene
Neogene
Temperature [°C]
Time [Ma]
P: 1.07 E+06;
Ac: 3976;
G: 1000;
He Zircon: Zircon Diffusional Profile
AD: 18.5 (1.5) Ma
AM: 18.5 Ma
G.O.F.: 0.99
Total He: 2.685e+1 nmol/g
He Apatite: Apatite Diffusional Profile
AD: 15.4 (0.9) Ma
AM: 15.4 Ma
G.O.F.: 0.98
Total He: 2.995e+1 nmol/g
Norm. Concentration
Normalized Radius

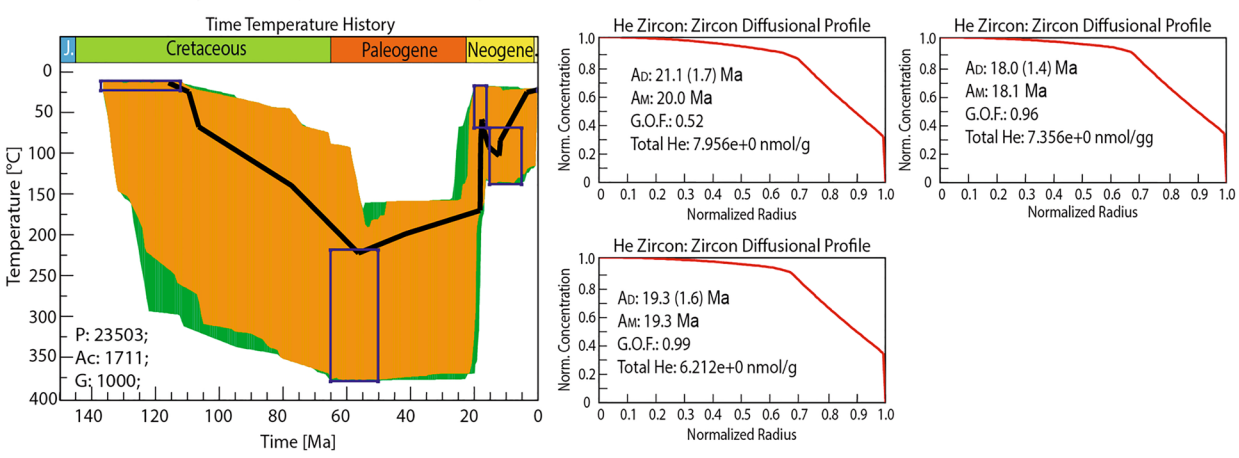
FU-06-07* (Sandstone, Lower Cretaceous)
Time Temperature History
J.
Cretaceous
Paleogene
Neogene
Temperature [°C]
Time [Ma]
P: 23503;
Ac: 1711;
G: 1000;
He Zircon: Zircon Diffusional Profile
AD: 21.1 (1.7) Ma
AM: 20.0 Ma
G.O.F.: 0.52
Total He: 7.956e+0 nmol/g
He Zircon: Zircon Diffusional Profile
AD: 18.0 (1.4) Ma
AM: 18.1 Ma
G.O.F.: 0.96
Total He: 7.356e+0 nmol/gg
He Zircon: Zircon Diffusional Profile
AD: 19.3 (1.6) Ma
AM: 19.3 Ma
G.O.F.: 0.99
Total He: 6.212e+0 nmol/g
Norm. Concentration
Normalized Radius

◂**Fig. 6** Thermal history models of Lower Cretaceous sandstone samples from the "West-Central Basal Complex" modelled using the software code HeFTy (Ketcham et al. 2007a, b, 2009). The left column displays the *t–T* paths, the right column displays the helium diffusion profile. For further information, please see Fig. 4

- 10.7 ± 0.9 Ma: AFT cooling ages close to the extrusion and intrusion age of the submarine pillow basalt (#Lag 1) and the pegmatitic gabbro (#Lag 8).
- av. 6.7 ± 1.6 Ma: AFT cooling ages of samples #Lag 3, 4, 5, and 6, rocks of the P1 suite, P2 suite, and P3 suite.
- 4.8 ± 0.7 Ma: AFT cooling ages of one trachyte dike (#Lag 9).

Thermal history (*t–T*) modelling

Two samples, the pillow basalt (#Lag 1) and the Tamargada monzonite (#Lag 3) revealed enough confined fission-track length to perform a numerical modelling of the *t–T* evolution (Fig. 10).

Pillow basalt: from a marine extrusion temperature at 11.5 ± 0.7 Ma the temperature increased to ~ 75 °C at 10.0 Ma. Thereafter, the temperature dropped rapidly reaching ~ 20 °C at ~ 9 Ma. Interesting enough the T increased again and reached a max. *T* of ~ 50 °C at 7 Ma. A second rapid decrease reaching surface *T* (20 °C) at about 6 Ma. The temperature kept at about 20 °C until recent.

Summarising the *t–T* evolution five major pattern is seen:

- at ~ 10 Ma reaching a maximum temperature of ~ 75 °C.
- at ~ 9 Ma rapid cooling to ~ 20 °C.
- at ~ 7 Ma reaching a new maximum *T* of ~ 50 °C.
- at ~ 6 Ma rapid decrease in *T* to surface temperature.

Tamargada monzonite: Following a fast cooling from more than 500–220 °C at ~ 9 Ma the *t–T* evolution gradual decrease reaching surface temperature recently.

Summarising the *t–T* evolution two major pattern are seen:

- at ~ 9 Ma rapid cooling from ~ 500 to 220 °C.
- gradual decrease of T to recent surface temperature.

Discussion and interpretation

Fuerteventura Island

Northwest Basal Complex

The "Northwest Basal Complex" comprises Upper Oligocene carbonatites, pyroxenites, Ijolites, and syenites, as well as layered and coarse-grained gabbros. The formation ages of carbonatites, pyroxenites, Ijolites, and Syenites range between 28.3 ± 0.2 Ma and 27.2 ± 0.4 Ma. Zircon and apatite fission-track ages are partly from the same samples displayed in a time–temperature diagram show a cooling path between formation age and ~ 19 Ma (Fig. 4). Thereafter, the complex must have been reheated to temperatures between 60 and 110 °C depending on the length of the heating period. The information that the Northwest Basal Complex has been at or near the surface at about 19 Ma was given by literature and the recent occurrence of relict volcanic rocks younger than 19 Ma partly overlying the complex. More detailed information is provided by the numerical modelling.

The modelled *t–T* evolution of the samples revealed a moderate cooling from ~ 500 to ~ 280 °C between the formation age and ~ 20 Ma (Fig. 5). A significant cooling occurred instantaneous around 20 Ma and rock temperature decreased from 280 to ~ 20 °C. Stillman (1999) proposed a giant landslide earlier than 18.3 Ma. Acosta et al. (2003) attributed the Puerto Rosario debris Avalanche offshore to have been caused by giant landslides older than 17.5 Ma (Fig. 1). Therefore, we assume that the rapid cooling path most likely reflects the rapid cooling caused by the instantaneous denudation of the large northern volcanic edifice forming part of the Puerto Rosario debris Avalanche offshore.

Following the rapid cooling at 20 Ma, the *t–T* evolution indicates a reheating from surface temperature to ~ 100 °C. Such an increase in temperature possibly implies the thermal influence of a newly formed volcanic edifice (the Northern Volcanic Complex) that superimposed the earlier rock formations. New volcanic activity might also increase the geothermal gradient. Therefore, the height of the new volcanic edifice cannot be calculated. Considering the published formation ages of the deposited volcanic rocks of the Northern Volcanic Complex (NCV), the NVC I with ages between 18.7 ± 0.3 and 15.3 ± 1.3 Ma and the volcanic rocks of the NCV-II with an av. age of 13.6 ± 0.8 Ma, would explain the increase in temperature. The apatite fission-track ages of av. 18.7 ± 2.4 Ma and 14.5 ± 2.9 Ma fall within this time interval, in general. Also, the AFT age (17.8 ± 5.0 Ma) of the Tindaya trachyte dome, which are within error the same as the published formation age falls within the time of reheating of the intrusive rocks. From ~ 14 Myrs on a slow cooling to 20 °C indicate a low erosion or/and decrease of the geothermal gradient leading to the recent surface exposure of the "Northwest Basal Complex".

West-Central Basal Complex

Lower Cretaceous sandstones, Upper Oligocene to Lower Miocene intrusions, basic dikes of a sheeted dike swarm, and various dikes represent the lithological units of the "West-Central Basal Complex". The formation of the sandstones range between 137 and 112 Ma and of the magmatic rocks

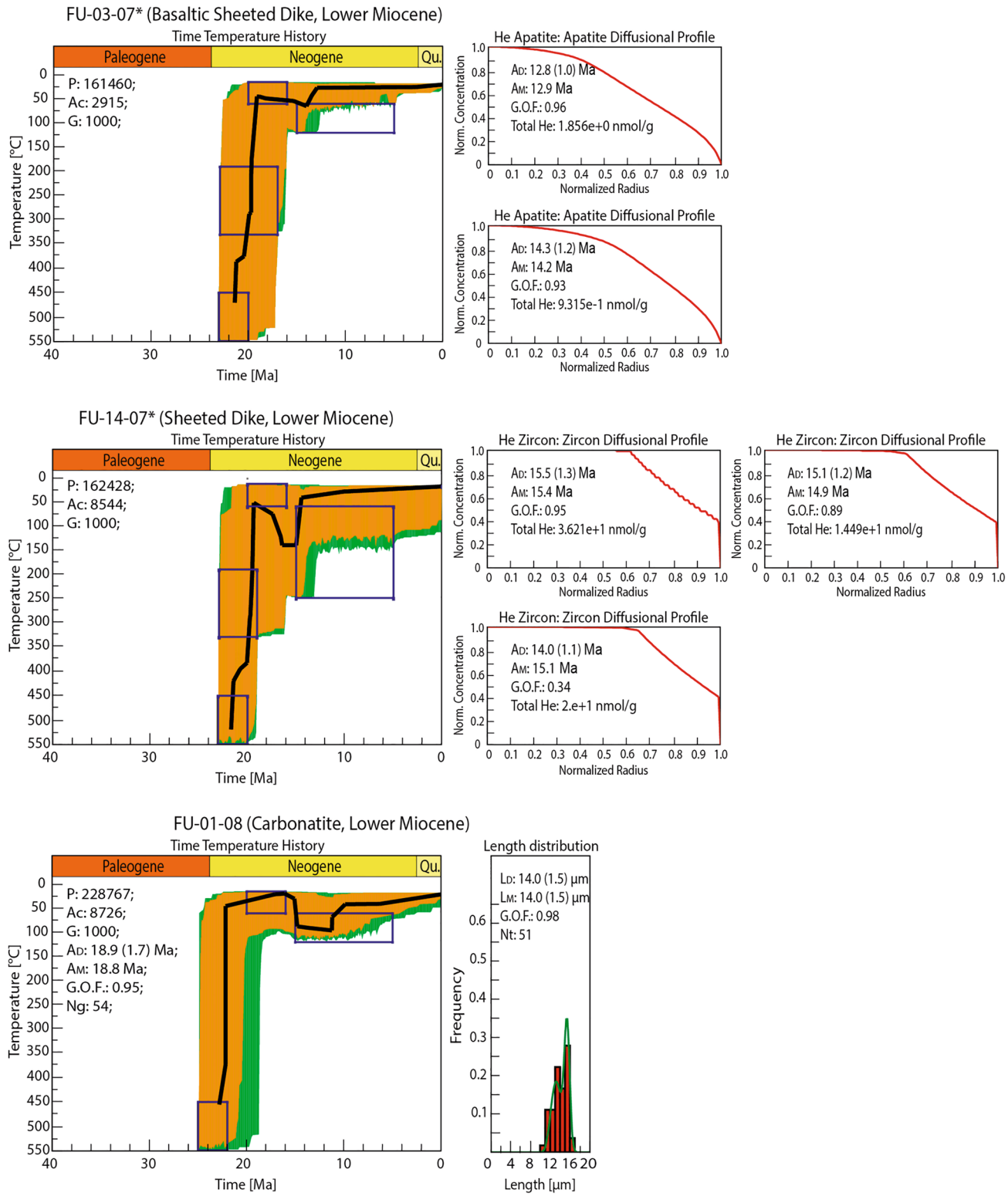

Fig. 7 Thermal history models of samples from the "West-Central Basal Complex" modelled using the software code HeFTy (Ketcham et al. 2007a, b, 2009). The left column displays the *t*–*T* paths, the right column displays the helium diffusion profile. For further information, please see Fig. 4

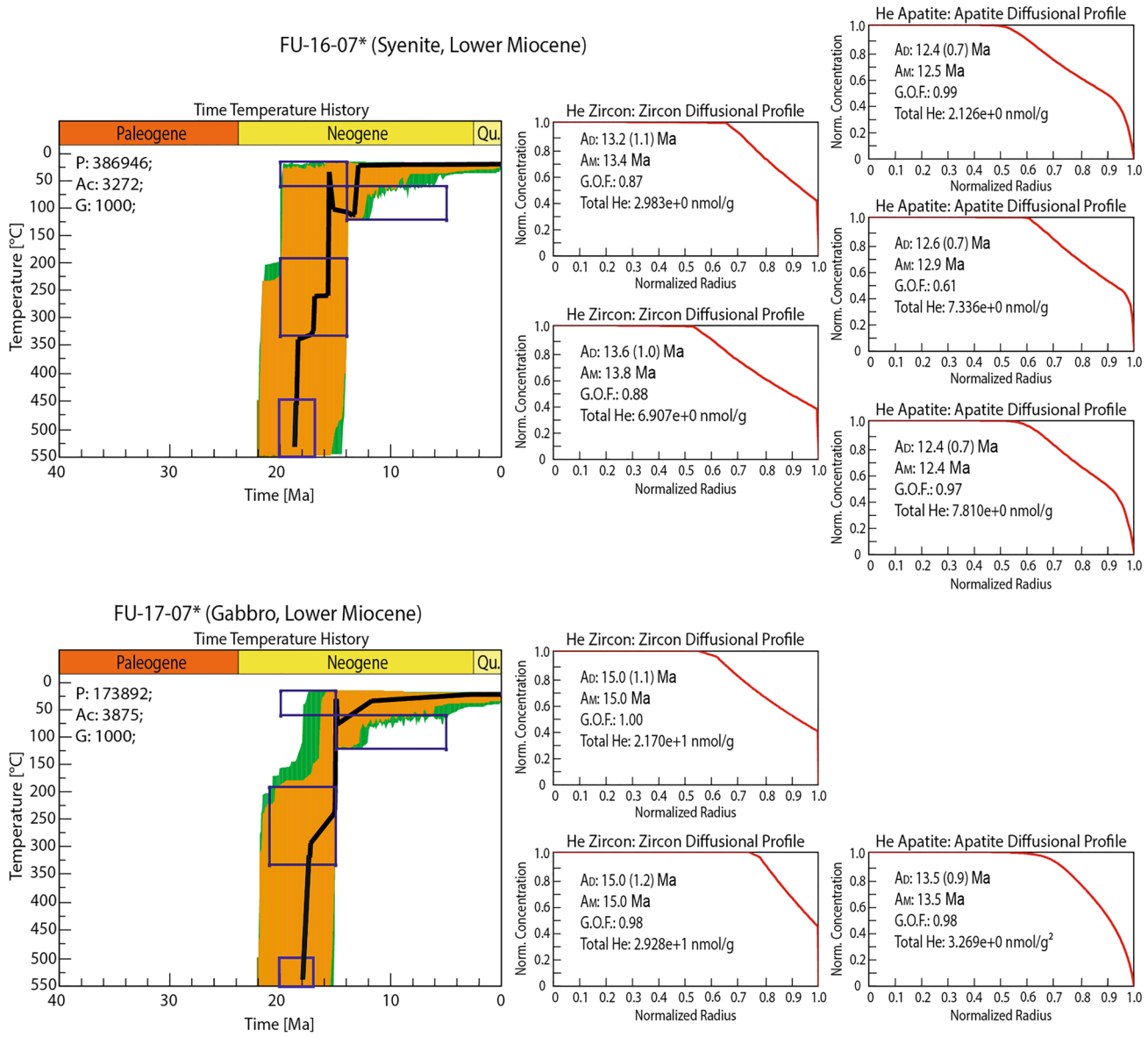

Fig. 8 Thermal history models of samples from the "East-Central Basal Complex" modelled using the software code HeFTy (Ketcham et al. 2007a, b, 2009). The left column displays the *t*–*T* paths, the right column displays the helium diffusion profile. For further information, please see Fig. 4

range between 26.2 ± 0.2 and 17 Ma (Fig. 4). Zircon and apatite fission-track and (U–Th)/He ages partly from single magmatic samples displayed in a time–temperature diagram show a cooling path between formation age and ~ 19 Ma (Fig. 4). Similarly, after a subsidence period reaching around 300 °C the sandstones cooled slowly to 200 °C at ~ 19 Ma and, thereafter, instantaneously to near surface temperatures. Towards younger time, the complex must have been reheated to temperatures between 60 and 110 °C depending on the length of the heating period. The information that the West-Central Basal Complex has been at or near the surface at about 19 Ma was given by literature and the recent occurrence of relict volcanic rocks younger than 19 Ma partly overlying the complex. More detailed information is provided by the numerical modelling.

The temperature evolution of the sandstones reached ~ 300 °C or more at ~ 55 Ma (Fig. 6). Such high temperature agrees with the published metamorphic grade of the Lower Cretaceous sedimentary rock series (Steiner et al. 1998). They termed that the sedimentary rock sequence was affected by thermal low greenschist grade to intermediate greenschist grade, and interpreted the thermal metamorphism as caused by the Oligocene to Miocene various intrusions and the sheeted dike swarm. Therefore, reaching the

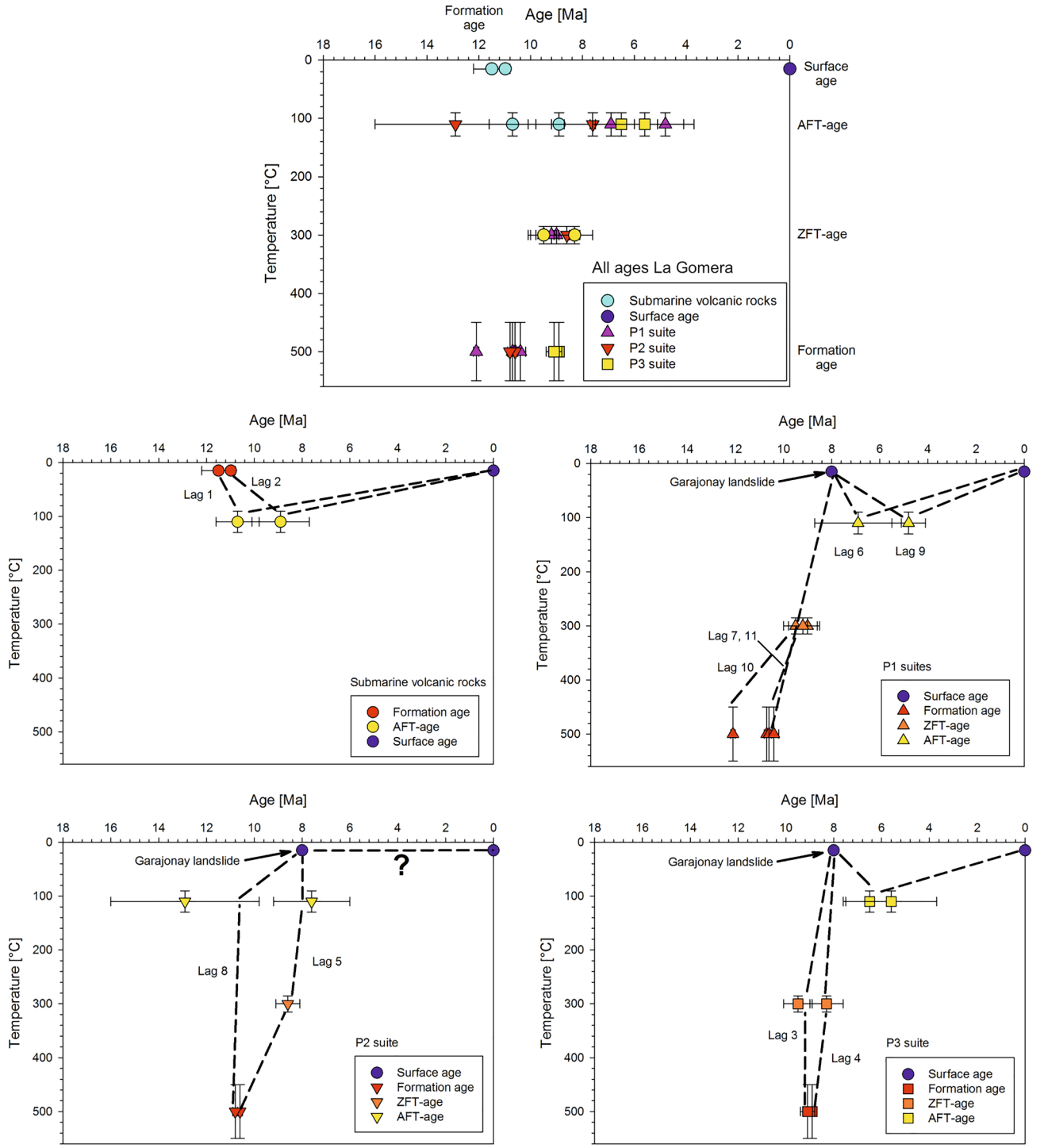

Fig. 9 Formation ages and Thermochronological ages of the four lithological units in La Gomera. Temperature according to the known final diffusion and annealing temperature at a cooling rate of 10 °C/Ma. The dashed lines represent possible cooling path between the thermochronological ages of individual samples

high temperature at ~ 55 Ma might be related to the start of the submarine growth stage of Fuerteventura with increased magmatic activity. The temperature decreased slowly reaching ~ 250 °C at 20 Ma. Thereafter, the temperature instantaneously decreased to a near surface temperature. Similarly, the *t*–*T* history of the carbonatite and the two basic dikes indicate a rapid cooling from formation temperature to near surface temperature at ~ 20 Ma (Fig. 7). Such

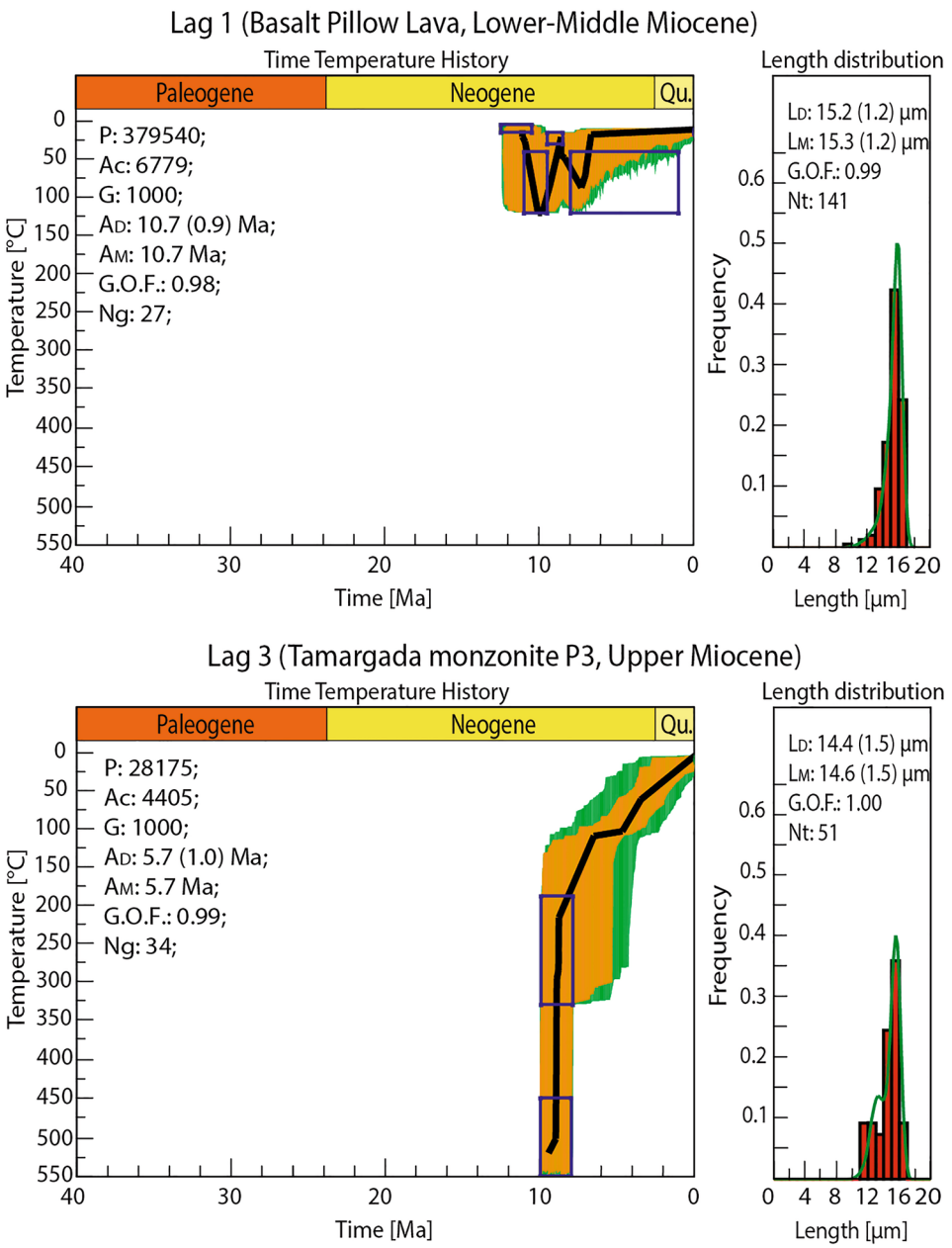

Fig. 10 Thermal history models of samples from La Gomera modelled using the software code HeFTy (Ketcham et al. 2007a, b, 2009). The left column displays the *t*–*T* paths, the right column displays the helium diffusion profile. Lag 1 are a sample of pillow lavas extruded to the ocean. For further information, please see Fig. 4

a rapid temperature decrease occurred at a similar time in the "Northwest Basal Complex". It seems to be likely, that the causes are similar. The rapid decrease in temperature might have been caused by the movement of a giant landslide leading to an instantaneous denudation of the volcanic edifice on top of the "Basal Complexes" and, therefore, to an instantaneous drop in temperature. We cannot exclude but also, we cannot assume that the giant landslide causing instantaneous erosion in the "Northwest Basal Complex" area and the giant landslide causing instantaneous erosion in the "West-Central Basal Complex" has occurred at the same time. It could also be within error of the dating and numerical modelling that the two giant landslide events occur separately. Part of the samples slowly cooled to recent surface temperatures. Whereas other samples were heated to a new temperature maximum between ~ 80 and ~ 115 °C at ~ 14 Ma and cooled rapidly to near surface temperature, thereafter. The T-increase is assumed to be related to the next generation (CVC I-III) of massive volcanic activity causing the formation of a new volcanic edifice (Central Volcanic Complex). The rapid cooling at ~ 14 Ma might also be related to a new formation of a landslide. The Pliocene evolution is documented in two NE–SW-trending trachytic dikes crossing the Upper Jurassic to Cretaceous sedimentary rocks of the "West-Central Basal Complex". However, as

noted above, these dikes are located close (tenth of metre) to a large Pliocene basaltic flow of the Series II. They might have been thermally influenced by the basaltic flow. Therefore, it cannot be excluded that the age might represent a reheating and, thereafter, fast cooling caused by the Pliocene basaltic flow.

East-Central Basal Complex Miocene syenite and gabbro intrusions ((“Vega de Rio Palmas Ring Complex”; Betancuria Complex) and a trachyte represent the analysed lithological units of the “East-Central Basal Complex”. The formation age of the one syenite and one gabbro intrusion (“Vega de Rio Palmas Ring Complex”) is 18.7 ± 0.8 Ma and 18.4 ± 0.3 Ma, respectively. Zircon and apatite fission-track and (U–Th)/He ages partly from single magmatic samples displayed in a time–temperature diagram show a rapid cooling path between formation age and ~ 18 Ma (Fig. 4). This decrease in temperature might be related to the crystallisation and cooling of the magma. Up to a temperature of about 75 °C the *t*–*T* path cools gradually and is followed by a slow cooling to surface temperature. More detailed information is provided by the numerical modelling.

The numerically modelled *t*–*T* path is constrained by the formation age, the thermochronological ages and the request for a near surface occurrence at ~ 16 Ma. Gabbros and syenites of the “Vega de Rio Palmas Ring Complex” are overlain by volcanic rocks of younger age. Both *t*–*T* path shows cooling from intrusion temperature to near surface temperatures between 18 and 16–15 Ma. In both cases, an increase in temperature is possible before the *t*–*T* path reached surface temperature at ~ 10–9 Ma.

Summarising, the giant landslide at ~ 20 to ~ 19 Ma is attributed to have led to the deposition of the offshore Puerto Rosario debris Avalanche that covers an area of about 3500 km^2 (Stillman 1999; Acosta et al. 2003; Fig. 1). The formation age of the Puerto Rosario debris Avalanche was provided by Acosta et al. (2003) with older than 17.5 Ma. Nevertheless, it remains highly uncertain whether only one giant landslide resulted in the formation of the debris avalanche unit, or it reflects a product of several repeatedly deposited debris flows (Acosta et al. 2003). The one of the “East-Central Basal Complex” at ~ 16 Ma to ~ 15 Ma might be of local origin. If the mass movement did not reach the ocean, it could be that the increase in temperature at that time in the “West-Central Basal complex” is related to the deposition of the landslide mass on top of the volcanic rocks of the “West-Central Basal Complex”.

What might have caused the initiation of the two landslides? The movement at ~ 20 Ma to ~ 19 Ma and at ~ 16 Ma to ~ 15 Ma might have been triggered by the **new volcanic activity** forming the North Volcanic and the Central Volcanic Complex (Coello et al. 1992; Ancochea et al. 1996). Therefore, the landslide might have been triggered by new volcanic activity on the Island. In addition, the **tectonic activity** that affected the Miocene Volcanic Complexes of Fuerteventura (Gutiérrez et al. 2006; Fernández et al. 2006) could have co-helped the formation of these large gravitational slides. A third possibility might be the **change in climate** leading to increase in seasonal rain. As within the Miocene two climate optimums (Zachos et al. 2001, 2008) exist, we cannot rule out the influence of climate change on the formation of the landslides. According to Hendriks et al. (2020) and Steinthorsdottir et al. (2021), the sea surface temperature in the region of the Canary Islands dropped rapidly at about 19 Ma. Therefore, we do not exclude an influence by climate change on the formation of the giant landslides.

La Gomera Island

The Basal Complex in La Gomera Island comprises Middle to Upper Miocene pillow basalts, submarine basaltic and trachytic hyaloclastite, amphibole gabbros, trachyte, amphibole pyroxenites, syenites, monzonites, and pegmatitic gabbros. The formation ages range between 12.1 ± 0.1 and 8.9 ± 0.1 Ma. As the formation age (11.5 ± 0.7 Ma) and the AFT age (10.7 ± 0.9 Ma) of the pillow basalt (#Lag 1) are the same within error, it is assumed that the AFT age does not represent a reheating event but displays the formation of the pillow basalt (Fig. 9). Nevertheless, we did used the numerical modelling to test if the difference of ages could have been caused by a reheating event (Fig. 10). The results indicate that the data set could be numerically modelled with a reheating event. The numerical modelling presented the result of a possible two reheating event. To decide between the two possibilities, age data with less error are needed. The sample representing the submarine trachytic breccia (#Lag 2) has an AFT age (8.9 ± 1.2 Ma) that is younger than the age range covered by the error of the formation age (10.98 ± 0.08 Ma). Therefore, it might be possible that the rock suite was thermally altered after the deposition either by an increase in heat flow, by overlain rocks or by both processes. The sample was taken from a unit that is located close to the Tazo landslide plane. According to Anchochea et al. (2006) and Casillas et al. (2010, 2011), the Tazo giant landslides have moved large masses of volcanic material in short time in the north-western sector of La Gomera. The movement of the Tazo landslide (Figs. 1, 2) has been dated at ~ 9.4 Ma, which is between the formation age of the submarine trachytic breccia, and the AFT age. Therefore, it could be possible that not all landslide material was moved into the ocean (Fig. 1) but was partly deposited above the submarine trachytic breccia, which would explain the younger apatite fission-track age.

All samples of P1 suite, P2 suite and P3 suite are in the area where the morphology has significant changed at ~ 8.0 Ma by the occurrence of the Garajonay caldera collapse followed by a fast removal of rocks (Paris et al. 2005; Rodriguez-Losadaa and Martinez-Frias 2004). According to Paris et al. (2005), we assumed that the Garajonay landslide caused the unravel of the rocks that were analysed in this study by moving a large volume of volcanic rocks (Fig. 9). Unfortunately, the ZFT- and AFT ages of the magmatic rocks taken from the "Basal complex" P1 suite are not from the same sample. The age difference between the formation age of the amphibole gabbro (#Lag 7, 10.6 ± 0.1 Ma), the amphibole pyroxenite (#Lag 10, 12.1 ± 0.1 Ma), and the trachytic dike (#Lag 11, 10.7 ± 0.1 Ma) and the ZFT ages (#Lag 7, 9.0 ± 0.5 Ma; #Lag 10, 9.5 ± 0.5 Ma; #Lag 11, 9.2 ± 0.6 Ma) indicate a differentiated fast cooling of the rocks from about 500 °C to about 300 °C. Thereafter, the rocks might have moved directly to the surface at ~ 8.0 Ma. One amphibole pyroxenite (#Lag 6; Form. age: 10.6 ± 0.1 Ma) and one trachytic dike (#Lag 9; Form. age: 10.4 ± 0.2 Ma) revealed only AFT ages (6.9 ± 1.8 Ma, 4.8 ± 0.7 Ma, respectively) but have within error similar formation ages as the samples #Lag 7 and #Lag 11.

The Lower Old Edifice P2 suite is represented by two samples a syenite dike (#Lag 5), and a pegmatitic gabbro (#Lag 8). The sample #Lag 8 is located close to the Garajonay landslide, whereas the sample #Lag 5 is further away. The temperature of sample #Lag 5 decreased gradually from 500 °C at 10.6 ± 0.1 Ma to 300 °C at 8.6 ± 0.5 Ma, and 110 °C at 7.6 ± 1.6 Ma (Fig. 9). We cannot exclude that the AFT age represents a reheating by post-Garajonay landslide intrusions or volcanic activity. In Fig. 9, we assumed a steady cooling path from high temperature to surface in a very short time. The thermochronological data of #Lag 8 revealed indicate a fast cooling from formation temperature (500 °C) at 10.8 ± 0.1 Ma to 110 °C at 12.9 ± 3.1 Ma. Within error, the formation age and the thermochronological age is the same. The Upper Old Edifice is represented by one monzonite sample (#Lag 3) and one syenite sample (#Lag 4) of the Tamargada Plutonic Complex. The formation age of the Tamargada monzonite (9.1 ± 0.3 Ma) and the Tamargada syenite (8.9 ± 0.1 Ma) are within error the same. Considering the thermochronological age distribution the monzonite and the syenite cooled fast from 500 °C at formation temperature to 300 °C at 9.5 ± 0.6 Ma and 8.3 ± 0.7 Ma and, thereafter, to surface temperatures at ~ 8.0 Ma (Fig. 9). The apatite fission-track ages (~ 110 °C) are much younger (6.5 ± 1.1 Ma; 5.6 ± 1.9 Ma) but within error are the same for the monzonite and the syenite indicating a new temperature increase of the intrusive rocks. More detailed information is gained by the numerical modelling (Fig. 10). We performed a numerical modelling with and without the occurrence of the Garajonay landslide. The results indicate that both *t–T* evolution paths are possible. The rapid cooling of the monzonite extends from ~ 500 to ~ 200 °C at ~ 9.0 Ma. Thereafter, the *t–T* path changed to an intermediate degree of cooling with a slight break at about 6 Ma.

Summarising the former results: the increase in temperature after formation of the pillow basalt might be related to the deposition of about 1.000 m of volcanic rocks above the pillow basalts. The calculation of the height of the volcanic edifice depends on the assumption of general geothermal gradient at about 10 Ma. Therefore, the thickness of the volcanic pile could have been less or more than 1000 m. In addition, Demény et al. (2010) showed that the green schist facies metamorphism of the Basal Complex of La Gomera was induced by the interaction with meteoric water. The inferred isotopic compositions of the meteoric water indicate that the water infiltrated the rocky building at an elevation of approximately 1500 m above sea level, suggesting the existence of a subaerial volcano that was formed during the intrusive activity and that has been denudated or remains buried by subsequent volcanic events and landslides. Therefore, the thickness of the volcanic pile could have been even more than 1000 m.

As mentioned by Anchochea et al. (2006) and Casillas et al. (2010, 2011), giant landslides such as the Tazo landslide in the north-western sector of La Gomera have moved large masses of volcanic material in short time, which was followed by longer times of stagnation. The movement of the Tazo landslide has been dated at ~ 9.4 Ma. This timing of mass movement falls together with the rapid cooling of the pillow basalt in the NW, and the intrusion of the Tamargada monzonite (8.9 ± 0.1 Ma) and syenite (9.1 ± 0.3 Ma). Casillas et al. (2010, 2011) and Fernández et al. (2015) relate the triggering of the Tazo landslide with the movement of the Guillama and Montaña de Alcalá faults, under the Lower Old edifice (LOE). However, it appears that the intrusion of monzonitic or syngenetic magma could also have co-assisted the occurrence of the Tazo landslide. The Tazo landslide possibly caused the offshore occurrence of the submarine debris avalanche (Segments I and VIII; Fig. 1). According to Anchochea et al. (2006), the Lower Old Edifice (LOE) formed during that time indicating a major phase of volcanic activity and, therefore, a high heat flow resulting in a high geothermal gradient. A height of up to 1900 m for the Lower Old Edifice volcano with a location in the general area of the Tamargada intrusive complex was discussed. Considering the published data, we assume a geothermal gradient of about 100 °C for rocks surrounding the monzonite. As motioned before, we cannot exclude the influence of climate change on the formation of the Tazo landslide. Böhme et al. (2003, 2008, 2011) and Henderiks et al. (2020) discuss a significant increase in humidity at about 9.0 Ma. It might be that the tectonic activity described by Casillas et al. (2010) and Fernández et al. (2015) at the Guillama and Montaña

de Alcalá faults combined with the intrusion of the Tamargada monzonite/syenite, and a higher precipitation have triggered the development of the Tazo landslide. Considering the occurrence of the Garajonay landslide at ~ 8.0 Ma, the samples of the P2 suite cooled to near surface temperatures. The *t*–*T* path between 8.0 Ma and recent is not constrained by thermochronological data. In contrast, the samples of the P1 suite and P3 suite indicate a temperature increase after the landslide occurred. This temperature increase could have been caused by new volcanic activity. Our data do not provide any evidence on what kind of process triggered the occurrence of the Garajonay landslide. If the movement of the Garajonay landslide occurred earlier, it might be related to the intrusion of the Tamargada monzonite and syenite.

Conclusion

The decay of volcanos on Volcanic Islands such as La Gomera and Fuerteventura is often related to the movement of giant landslides causing the formation of submarine debris avalanches, and eventually Tsunamis. Dating the movement of such landslides would increase the understanding of the possible causes that trigger the movement, and furthermore might provide a hint to Tsunami formation over time. Younger formation of landslides can be dated by luminescence or electron spin resonance dating. If organic particles are involved even ^{14}C-dating might be a technique to reveal the age of the movement. However, all this dating techniques can only be applied to an age range between recent and about 2 Ma (electron spin resonance dating). If the sliding plan has been heated to a temperature that generated a melt and K-minerals are crystallised out of the melt on the plane surface K–Ar or even ^{40}Ar/^{39}Ar-dating could be applied. Low-temperature thermochronological dating techniques such as fission-track dating and (U–Th)/He dating have the advantage to reveal a *t*–*T* cooling/exhumation path of magmatic rocks that were below a certain pile of volcanic rocks before the instantaneous movement of the overlain rock pile. Therefore, this study tested the possibility of dating landslides by thermochronological tools using the cooling/exhumation history of the magmatic rocks. Our research could provide evidence that the proposed giant landslide (Stillman 1999) leading to destruction of the Northern Volcanic Complex and the central Volcanic complex occurred at ~ 20 Ma on Fuerteventura. Furthermore, we identified a possible second movement of volcanic rocks at about 16 Ma in the "East-Central Basal Complex" of Fuerteventura. Two landslides are described for La Gomera. The Tazo landslide formed at ~ 9.4 Ma (Casillas et al. 2010, 2011) and the Garajonay landslide formed at ~ 8.0 Ma (Paris et al. 2005; Rodriguez-Losadaa and Martinez-Frias 2004). The thermochronological data presented in this paper provide evidence for the movement of both landslides. Summarising the research, it is possible to date landslides on volcanic Islands with thermochronological data. Furthermore, if the palaeo geothermal gradient is known, a numerically gained cooling path can be transferred into the thickness of the rock mass moved by the landslide.

Supplementary Information The online version contains supplementary material available at https://doi.org/10.1007/s00531-022-02253-7.

Acknowledgements The first author was financially supported by a cooperation scholarship between the Egyptian ministry of higher education (MoHE) and the Deutscher Akademischer Austauschdienst (DAAD). This work has also benefited from financial support of the research projects BTE 2003-00569 y CGL 2006-00970/BTE (Spanish Ministry of Education and Culture, MEC); CGL2009-07775 (Spanish Ministry of Competitiveness and Innovation, MCI), CGL2016-75062-P (Spanish Ministry of Science and Innovation), PID2020-112920GB-I00 (Spanish Ministry of Science and Innovation), and 2008/0250 (Agencia Canaria de Investigación, Innovación y Sociedad de la Información del Gobierno de Canarias). It forms part of the activities of the University of La Laguna Search Group "Crecimiento submarino émersion de las Islas Canarias: estudio geológico de los Complejos Basales". We also like to thank the reviewers for their constructive comments and suggestions.

Funding Open Access funding enabled and organized by Projekt DEAL.

References

Abdel Monen A, Watkins ND, Gast PW (1971) Potassium–argon ages, volcanic stratigraphy, and geomagnetic polarity history of the Canary Islands: Lanzarote, Fuerteventura, Gran Canaria and La Gomera. Am J Sci 271:490–521

Abu El-Rus MA, Neumann ER, Peters V (2006) Serpentinization and dehydration in the upper mantle beneath Fuerteventura (eastern Canary Islands): evidence from mantle xenoliths. Lithos 89:24–46

Acosta J, Uchupi E, Muñoz A, Herranz P, Palomo C, Ballesteros M, ZEE Working Group (2003) Geologic evolution of the Canarian Islands of Lanzarote, Fuerteventura, Gran Canaria and La Gomera and comparison of landslides at these islands with those at Tenerife, La Palma and El Hierro. Marine Geophys Res 24:1–40https://doi.org/10.1007/s11001-004-1513-3

Allibon J, Bussy F, Lewin É, Darbellay B (2011a) The tectonically controlled emplacement of a vertically sheeted

gabbro-pyroxenite intrusion: Feeder-zone of an ocean-island volcano (Fuerteventura, Canary Islands). Tectonophysics 500:78–97

Allibon J, Ovtcharova M, Bussy F, Cosca M, Schaltegger U, Bussien D, Lewin É (2011b) Lifetime of an ocean island volcano feeder zone: constraints from U-Pb dating on coexisting zircon and baddeleyite, and $^{40}Ar/^{39}Ar$ age determinations, Fuerteventura, Canary Islands. Can J Earth Sci. https://doi.org/10.1139/E10-032

Ancochea E, Brändle JL, Cubas CR, Hernán F, Huertas MJ (1996) Volcanic complexes in the eastern ridge of the Canary Islands: the Miocene activity of the Island of Fuerteventura. J Volcanol Geotherm Res 70:183–204

Ancochea E, Brändle JL, Huertas MJ, Cubas CR, Hernán F (2003) The felsic dikes of La Gomera (Canary Islands): identification of cone sheet and radial dike swarms. J Volcanol Geotherm Res 120:197–206

Ancochea E, Hernán F, Huertas MJ, Brändle JL, Herrera R (2006) A new chronostratigraphical and evolutionary model for La Gomera: implications for the overall evolution of the Canarian Archipelago. J Volcanol Geotherm Res 157:271–293

Ancochea E, Brändle JL, Huertas MJ, Hernán F, Herrera R (2008) Dike-swarms, key to the reconstruction of major volcanic edifices: the basic dikes of La Gomera (Canary Islands). J Volcanol Geotherm Res 173:207–216

Anguita F, Hernán F (1975) A propagating fracture model versus a hotspot origin for the Canary Islands. EPSL 27:11–19

Araña V, Ortis R (1991) The Canary Islands: tectonics, magmatism and geodynamic framework. In: Kampunzu AB, Lubala RT (eds) Magmatism in extensional structural settings (The Phanerozoic African Plate). Springer, Barcelona, pp 209–249

Balogh K, Ahijado A, Casillas R, Fernández C (1999) Contributions to the chronology of the Basal Complex of Fuerteventura, Canary Islands. J Volcanol Geotherm Res 90:81–101

Barbarand J, Carter A, Wood IG, Hurford AJ (2003) Compositional and structural control of fission track annealing in apatite. Chem Geol 198:107–137

Beucher R, Roderick W, Brown RW, Roper S, Stuart F, Persano C (2013) Natural age dispersion arising from the analysis of broken crystals: Part II. Practical application to apatite (U–Th)/He thermochronometry. Geochem Cosmochim Acta 120:395–416

Boulestix T, Hildenbrand A, Soler V, Quidelleur X, Gillot P-Y (2013) Coeval giant landslides in the Canary Islands: implications for global, regional and local triggers of giant flank collapses on oceanic volcanoes. J Volcanol Geotherm Res 257:90–98

Böhme M (2003) The Miocene Climatic Optimum: evidence from ectothermic vertebrates of Central Europe. Palaeogeogr Palaeoclimatol Palaeoecol 195:389–401

Böhme M, Ilg A, Winklhofer M (2008) Late Miocene "washhouse" climate in Europe. EPSL 275:393–401

Böhme M, Winklhofer M, Ilg A (2011) Miocene precipitation in Europe: temporal trends and spatial gradients. Palaeogeogr Palaeoclimatol Palaeoecol 304:212–218

Bravo T (1964) Estudio geológico y petrográfico de la isla de isla de la Gomera I. Estudio Geológico Estudios Geológicos 20:1–21

Brix MR, Stockhert B, Seidel E, Theye T, Thomson SN, Küster M (2002) Thermobarometric data from a fossil zircon partial annealing zone in high pressure–low temperature rocks of eastern and central Crete, Greece. Tectonophysics 349:309–326

Brown RW, Beucher R, Roper S, Persano C, Stuart F, Fitzgerald P (2013) Natural age dispersion arising from the analysis of broken crystals: Part I. Theoretical basis and implications for the apatite (U–Th)/He thermochronometer. Geochem Cosmochim Acta 121:478–497

Burke K, Wilson JT (1972) Is the African plate stationary? Nature 239:387–390

Burtner RL, Nigrini A, Donelick RA (1994) Thermochronology of lower Cretaceous source rocks in the Idaho-Wyoming thrust belt. AAPG Bull 78:1613–1636

Cantagrel JM, Cendrero A, Fúster JM, Ibarrola E, Jamond C (1984) K–Ar chronology of the volcanic eruption in the Canarian Archipelago: Island of La Gomera. Bull Volcano 47:597–609

Cantagrel JM, Fúster JM, Pin C, Renaud U, Ibarrola E (1993) Age Miocène inférieur des carbonatites de Fuerteventura (23 Ma: U–Pb zircon) et le magmatisme prècoce d'une ile ocèanique (Ile Canaries). Comptes Rendues De L'academie Des Sciences Paris 316:1147–1153

Carlino S (2018) Heat flow and geothermal gradients of the Campania region (Southern Italy) and their relationship to volcanism and tectonic. J Volcanol Geotherm Res 365:23–37

Carnevale G, Caracausi A, Correale A, Italiano L, Rotolo SG (2021) An overview of the geochemical characteristics of oceanic carbonatites: new insights from fuerteventura carbonatites (Canary Islands). Minerals 11:203. https://doi.org/10.3390/min11020203

Carracedo JC (1996) A simple model for the genesis of large gravitational landslide hazards in the Canary Islands. In: McGuire WJ, Jones AP, Neuberg J (eds) Volcano instability on the earth and terrestrial planets. Geol Soc Lond, Spec Pub 110, pp 125–135

Carracedo JC, Day S, Gillou H, Rodríguez E, Canas JA, Pérez FJ (1998) Hotspot volcanism close to a passive continental margin. Geol Mag 135:591–604

Casillas R, Nagy G, Demény A, Ahijado A, Fernández C (2008a) Cuspidine-niocalite-baghdadite solid solutions in the metacarbonatites of the Basal Complex of Fuerteventura (Canary Islands). Lithos 105:25–41

Casillas R, Fernández C, De la Nuez J, García Navarro E, Colmenero JR, Martín MC (2008b) Deformaciones asociadas al deslizamiento gravitacional de flanco del Edificio Antiguo Inferior en Tazo (La Gomera). Geotemas 10:1269–1272

Casillas R, De la Nuez J, Fernández C, García-Navarro E, Colmenero JR, Martín MC (2008c) La secuencia volcánica submarina del Complejo Basal de La Gomera. Geotemas 10:1273–1276

Casillas R, Fernández C, Colmenero JR, de la Nuez J, García-Navarro E, Martín MC (2010) Deformation structures associated with the Tazo landslide (La Gomera, Canary Islands). Bull Volcano 72:945–960. https://doi.org/10.1007/s00445-010-0373-8

Casillas R, Colmenero JR, De la Nuez J, Fernández C (2011) Deposits associated with giant gravitational landslides of the flanks of the volcanic edifices of the Canary Islands: Examples of La Gomera, La Palma and Fuerteventura. In: Abstracts, 28th IAS meeting of sedimentology, Zaragoza, Spain (Eds. B. Bádenas, M. Aurell and A.M. Alonso-Zarza), p 343

Casillas R (2022) Internal Report on U-Pb-ages of zircon of Fuerteventura and La Gomera Island Basal Complex rocks (Canary Island). ULL, p 30

Cendrero A (1970) The volcano-plutonic complex of La Gomera (Canary Islands). Bull Volcano 34:537–561

Cendrero A (1971) Estudio geológico y petrológico del Complejo Basal de la Isla de La Gomera (Islas Canarias). Estud Geol 27:3–73

Clift PD (2010) Enhanced globalcontinental erosion and exhumation driven by Oligo-Miocene climate change. Geophys Res Lett 37:L09402. https://doi.org/10.1029/2010GL043067

Coello J, Cantagrel JM, Hernán F, Fúster JM, Ibarrola E, Ancochea E, Casquet C, Jamond JR, Cendrero A (1992) Evolution of the eastern volcanic ridge of the Canary Islands based on new K–Ar data. J Volcanol Geotherm Res 53:251–274

Coello-Bravo JJ, Márquez A, Raquel Herrera R, Huertas MJ, Ancochea E (2020) Multiple related flank collapses on volcanic oceanic islands: evidence from the debris avalanche deposits in the Orotava Valley water galleries (Tenerife, Canary Islands). J Volcanol Geotherm Res 401:106980. https://doi.org/10.1016/j.jvolgeores.2020.106980

Cohen KM, Finney SC, Gibbard PL, Fan JX (2013) The ICS International Chronostratigraphic Chart. Episodes 36:199–204. https://doi.org/10.18814/epiiugs/2013/v36i3/002

Cubas CR (1978) Estudio de los domos sa.licos de la isla de La Gomera (Islas Canarias). I. Vulcanología. Est Geol 34:53–70

Cubas CR, Hernán F, Ancochea E, Brändle JL, Huertas MJ (1994) Serie Basáltica Antigua Inferior en el sector de Hermigua, Isla de la Gomera. Geogaceta 16:15–18

Demény A, Ahijado A, Casillas R, Vennemann TW (1998) Crustal contamination and fluid/rock interaction in the carbonatites of Fuerteventura (Canary Islands, Spain); a C, O, H isotope study. Lithos 44:101–115

Demény A, Venneman TW, Hegner E, Ahijado A, Casillas R, Nagy G, Homonnay Z, Gutierrez M, Cs S (2004) H, O, Sr, Nd, and Pb isotopic evidence for recycled oceanic crust in the Transitional Volcanic Group of Fuerteventura, Canary Islands, Spain. Chem Geol 205:37–54

Demény A, Casillas R, Hegner E, Vennemann TW, Nagy G, Sipos P (2010) Geochemical and H-O-Sr-Nd isotope evidence for magmatic processes and meteoric-water interactions in the Basal Complex of La Gomera, Canary Islands. Min Pet 98:181–195. https://doi.org/10.1007/s00710-009-0071-4

Dodson MH (1973) Closure temperature in cooling geochronological and petrological systems. Cont Min Pet 40:259–274

Donelick RA, Miller DS (1991) Enhanced TINT fission track densities in low spontaneous track density apatites using ^{252}Cf derived fission fragment tracks: a model and experimental observations. Nucl Tracks Rad Meas 18:301–307

Donelick RA, Ketcham RA, Carlson WD (1999) Variability of apatite fission track annealing kinetics II: crystallographic orientation effects. Am Min 84:1224–1234

Donelick RA, O'Sullivan PB, Ketcham RA (2005) Apatite fission track analysis. Rev Min Geochem 58:49–94

Dunkl I (2002) Trackkey: a Windows program for calculation and graphical presentation of fission track data. Comp Geos 28:3–12

Elsworth D, Day SJ (1999) Flank collapse triggered by intrusion: the Canarian and Cape Verde Archipelagos. J Volcanol Geotherm Res 94:323–340

Farley KA, Wolf RA, Silver LT (1996) The effects of long alpha-stopping distances on (U–Th)/He ages. Geochem Cosmochim Acta 60:4223–4229

Farley KA (2000) Helium diffusion from apatite: general behaviour as illustrated by Durango fluorapatite. J Geophys 105:2903–2914

Féraud G, Giannerini G, Campredon R, Stillman CJ (1985) Geochronology of some Canarian dyke swarms: contributions to the tectonic evolution of the archipelago. J Volc Geotherm Res 25:29–52

Fernández C, Casillas R, Garcia NE, Gutierrez M, Camacho MA, Ahijado A (2006) Miocene rifting of Fuerteventura (Canary Islands). Tectonics 25:TC6005. https://doi.org/10.1029/2005TC001941

Fernández C, Casillas R, de la Nuez J, Garcia NE, Camacho MA (2015) Deformation of the substratum of a large shield volcano: triggering factor for past flank collapses in the old volcanic edifice of La Gomera, Canary Islands. GSA Bull 127:443–463. https://doi.org/10.1130/B30971.1

Flowers RM, Ketcham RA, Shuster DL, Farley KA (2009) Apatite (U–Th)/He thermochronometry using a radiation damage accumulation and annealing model. Geochem Cosmochim Acta 73:2347–2365

Fullea J, Camachoa AG, Negredo AM, Fernándeza J (2015) The Canary Islands hot spot: New insights from 3D coupled geophysical–petrological modelling of the lithosphere and uppermost mantle. EPSL 409:71–88

Fúster JM, Aguilar M (1965) Nota previa sobre la geología del Macizo de Betancuria, Fuerteventura Islas Canarias. Estudio Geológico 21:181–197

Fúster JM, Cendrero A, Gastesi P, Ibarrola E, Lopez Ruiz J (1968) Geología y Volcanología de las Islas Canarias – Fuerteventura. Institut 'Lucas Mallada', Consejo Superior de Investigationes Cientificas, Madrid, p 239

Fúster JM, Muñoz M, Sagredo J, Yebenes A, Bravo T, Hernández Pacheco A (1980) Excursión 121 A+C del 26 I.G.C. a las Islas Canarias. Boletín Geológico y Minero De España 91:351–390

Galbraith RF (1981) On statistical models for fission track counts. Math Geol 13:471–478

Garver JI (2003) Discussion: "Metamictization of natural zircon: accumulation versus thermal annealing of radioactivity-induced damage. Cont Min Pet 143:756–757

Garver JI, Kamp PJJ (2002) Integration of zircon color and zircon fission track zonation patterns in Orogenic belts: application of the Southern Alps, New Zealand. Tectonophysics 349:203–219

Gleadow AJW, Duddy IR (1981) A natural long term track annealing experiment for apatite. Nucl Tracks 5:169–174

Green P, Duddy I (2018) Apatite (U–Th–Sm)/He thermochronology on the wrong side of the tracks. Chem Geol 488:21–33

Guenther WR, Reiners PW, Ketcham RA, Nasdala L, Giester G (2013) Helium diffusion in natural zircon: radiation damage, anisotropy, and the interpretation of zircon (U–Th)/He thermochronology. Am J Sci 313:145–198

Gutiérrez M (2000) Estudio petrológico, geoquímico y émersion de la serie volcánica submarina del Complejo Basal de Fuerteventura (Islas Canarias): caracterización del crecimient émersion y de la émersion de la Isla. Ph.D. thesis. Universidad de La Laguna. Spain, p 553

Gutiérrez M, Casillas R, Fernández C, Balogh K, Ahijado A, Castillo C, Colmenero JR, García-Navarro E (2006) The submarine volcanic succession of the Basal Complex of Fuerteventura, Canary Islands: a model of submarine growth and emersion of some tectonic volcanic islands. GSA Bull 118:785–804

Henderiks J, Bartol M, Pige N, Karatsolis BT, Lougheed BC (2020) Shifts in phytoplankton composition and stepwise climate change during the middle Miocene. Paleoceanogr Paleoclimatol 35:e2020PA003915. https://doi.org/10.1029/2020PA003915

Herrera R, Huertas MJ, Ancochea E (2008) Edades 40Ar–39Ar del Complejo Basal de la isla de La Gomera. Geogaceta 44:7–10

Hoernle K, Tilton G (1991) Sr–Nd–Pb isotope data for Fuerteventura (Canary Islands) basal complex and subaerial volcanics: applications to magma genesis and evolution. Schweiz Min Pet Mitt 71:3–18

Hoernle K, Schmincke H-U (1993) The role of partial melting in the 15-Ma geochemical evolution of Gran Canaria: a blob model for the Canarian hotspot. Geotechnology 10:19–32

Hoernle K, Tilton G, Le Bas MJ, Duggen S, Garbe-Schönberg D (2002) Geochemistry of oceanic carbonatites compared with continental carbonatites: mantle recycling of oceanic crustal carbonate. Cont Min Pet 142:520–542

Holcomb RT, Searle RC (1991) Large landslides from oceanic volcanoes. Mar Geotechnol 10:19–32

Hurford AJ (1986) Standardization of fission track dating calibration: results of questionnaire distributed by international union of geological sciences subcommission on geochronology. Nuclear Tracks Rad Meas 11:329–333

Ibarrola E, Fúster JM, Cantagre JM (1989a) Evades K–Ar de las rotas volctiicas submarinas en el sector norte del Complejo Basal de Fuerteventura. E.S.F. Meet. Canarian Volcanism, pp 124–129

Ibarrola E, Ancochea E, Casquet, C, Fúster JM, Hernan F, Cendrero A, Diaz de Teran JR, Cantagrel JM, Jamond C (1989b) Cronoestratigrafia de las series volcánicas postmiocenas de la Isla de Fuerteventura. E.S.F. Mtg. Canarian Volcanism, Abstract, pp 134–138

IGME: Instituto Geológico y Minero de España (1991a) Geotermia, Estudios locales de detalle. http://www.igme.es/Geotermia/IGMEEstudioslocales.htm. Retrieved 10 July 2022

IGME: Instituto Geológico y Minero de España (1991b) Estudio Geotérmico de las Cañadas del Teide. http://www.igme.es/Geotermia/IGMEEstudioslocales.htm. Retrieved 10 July 2022

de Ignacio C, Muñoz M, Sagredo J, Barbero L (2002) Preliminary apatite-fission track geochronology of the Montaña Blanca-Milocho, alkaline pluton, (NW Fuerteventura, Canary Islands, Spain). Geotemas 4:54–59

Inokuchi T (1988) Gigantic landslides and debris avalanches on volcanoes in Japan. In: Proceedings of the Kagoshima international conference on volcanoes. National Institute for Research Administration, Japan, pp 456–459

Iverson RM (1991) Failure and runout of giant landslides on Hawaiian volcanoes: cases of enigmatic mechanics? GSA Abstr Progr 47:A125

Iverson RM (1995) Can magma-injection and groundwater forces cause massive landslides on Hawaiian volcanoes? J Volcanol Geotherm Res 66:295–308

Jonckheere J, Enkelmann E, Min M, Trautmann C, Ratschbacher L (2007) Confined fission tracks in ion-irradiated and step-etched prismatic sections of Durango apatite. Chem Geol 242:202–217

Karl M, Glasmacher UA, Kollenz S, Franco-Magalhaes AOB, Stockli DF, Hackspacher P (2013) Evolution of the South Atlantic passive continental margin in southern Brazil derived from zircon and apatite (U–Th–Sm)/He andfission-track data. Tectonophysics 604:224–244

King SD, Anderson DL (1998) Edge-driven convection. EPSL 160:289–296

Ketcham RA (2005) Forward and Inverse Modelling of low-temperature thermochronometry data. In: Reiners PW, Ehlers TA (eds) Low-temperature thermochronology: techniques, interpretations and applications. Rev Min Geochem 58:275–314

Ketcham RA (2017) HeFTy Version 1.9.3, manual, p 85

Ketcham RA, Carter A, Donelick RA, Barbarand J, Hurford AJ (2007a) Improved modelling of fission-track annealing in apatite. Am Mineral 92:799–810

Ketcham RA, Carter A, Donelick RA, Barbarand J, Hurford AJ (2007b) Improved measurements of fission-track annealing in apatite. Am Min 92:789–798

Ketcham RA, Donelick RA, Balestrieri ML, Zattin M (2009) Reproducibility of apatite fission-track length data and thermal history reconstruction. EPSL 284:504–515

Krastel S, Schmincke H-U, Jacobs CL, Rihm R, Le Bas TP, Alibe´s B, (2001) Submarine landslides around the Canary Islands. J Geophy Res 106:3977–3997

Lee HJ (2009) Timing of occurrence of large submarine landslides on the Atlantic Ocean margin. Mar Geol 264:53–64

Le Bas MJ, Rex DC, Stillman CJ (1986) The early magmatic chronology of Fuerteventura. Geol Mag 123:287–298

Lipman PW, Normark WR, Moore JG, Wilson JB, Gutmacher CE (1988) The giant Alika debris slide, Mauna Loa. Hawaii J Geophys Res 93:4279–4299

Mansour S (2015) Long-term topographic evolution of the African plate causes and consequences for surrounding lithospheric plates. Doctoral thesis, University Heidelberg, p 243

Marques FO, Hildenbrand A, Victória SS, Cunha C, Dias P (2019) Caldera or flank collapse in the Fogo volcano? What age? Consequences for risk assessment in volcanic islands. J Volcanol Geotherm Res 388:106686. https://doi.org/10.1016/j.jvolgeores.2019.106686

Márquez A, Herrara R, Izquierdo T, Martin-González F, López I, Martin-Velázquez (2018) The dyke swarms of the Old Volcanic Edifice of La Gomera (Canary Islands): implications for the origin and evolution of the volcanic rifts in oceanic island volcanoes. Glob Planet Change 171:255–272. https://doi.org/10.1016/j.gloplacha.2017.12.004

Masson DG (1996) Catastrophic collapse of the volcanic island of Hierro 15 ka ago and the history of landslides in the Canary Islands. Geology 24:231–234

Masson DG, Watts AB, Gee MJR, Urgeles R, Mitchell NC, Le Bas TP, Canals M (2002) Slope failures on the flanks of the western Canary Islands. Earth Sci Rev 57:1–35

McGuire WJ (1996) Volcano instability: a review of contemporary themes. In: McGuire WJ, Jones AP, Neuberg J (eds) Volcano Instability on the earth and terrestrial planets. Geological Society of London, Spec Publ 110, p 1–23

Miller MS, O´Driscoll LJ, Butcher AJ, Thomas C (2015) Imaging canary Island hotspot material beneath the lithosphere of Morocco and southern Spain. EPSL 431:186–194, https://doi.org/10.1016/j.epsl.2015.09.026

Moore JG (1964) Giant submarine landslides on the Hawaiian Ridge: US. Geological Survey Professional Paper 501-D:95–98

Moore JG, Clague DA, Holcomb RT, Lipman PW, Normark WR, Torresan ME (1989) Prodigious submarine landslides on the Hawaiian Ridge. J Geophys Res 94:17465–17484

Moore JG, Normark WR, Holcomb RT (1994) Giant Hawaiian landslides. An Rev Earth Planet Sci 22:119–144

Muñoz M (1969) Estudio petroldgico de las formaciones alcalinas de Fuerteventura, Islas Canarias. Estud Geol 25:257–310

Muñoz M, Sagredo J, Ignacio de C (2003) Field trip guide: Fuerteventura. IV EuroCarb workshop, Canary Islands, Spain, p 83

Muñoz M, Sagredo J, de Ignacio C, Fernández-Suárez J, Jeffries TE (2005) New data (U–Pb, K–Ar) on the geochronology of the alkaline-carbonatitic association of Fuerteventura, Canary Islands. Spain Lithos 85:140–153

Oehler J-F, van Wyk de Vries B, Laboratoire, PL (2005) Landslides and spreading of oceanic hot-spot and arc shield volcanoes on Low Strength Layers (LSLs): an analogue modelling approach. J Volcanol Geotherm Res 144:169–189

Paris R, Guillou H, Carracedo JC, Pérez-Torrado FJ (2005) Volcanic and morphological evolution of La Gomera (Canary Islands), based on new K–Ar ages and magnetic stratigraphy: implications for oceanic island evolution. J Geol Soc London 162:501–512

Rahn MK, Brandon MT, Batt GE, Garver JI (2004) A zero-damage model for fission track annealing in zircon. Am Min 89:473–484

Reiners PW, Brandon MT (2006) Using thermochronology to understand orogenetic erosion. An Rev Earth Planet Sci 34:419–466

Reiners PW, Farley KA, Hickes HJ (2002) He diffusion and (U–Th)/He thermochronometry of zircon: initial results from fish canyon tuff and gold butte, Nevada. Tectonophysics 349:297–308

Reiners PW, Spell TL, Nicolescu S, Zanetti KA (2004) Zircon (U–Th)/He thermochronometry: He diffusion and comparisons with 40Ar/39Ar dating. Geochem Cosmochim Acta 68:1857–1887

Renz O, Bernoulli D, Hottinger L (1992) Cretaceous ammonites from Fuerteventura, Canary Islands. Geol Mag 129:1–7

Robertson AHF, Stillman CJ (1979a) Late sedimentary rocks of Fuerteventura, Canary Islands. Implications for West African continental margin evolution. J Geol Soc Lond 136:47–60

Robertson AHF, Stillman CJ (1979b) Submarine volcanic and associated sedimentary rocks of the Fuerteventura Basal Complex, Canary Islands. Geol Mag 116:203–214

Robertson AHF, Bernouilli D (1982) Stratigraphy, facies and significance of Late Mesozoic and early Tertiary sedimentary rocks of Fuerteventura (Canary Islands) and Maio (Cape Verde Islands). In: Von Rad U et al (eds) Geology of the Northwest African Continental Margin. Springer, New York, pp 498–525

Rodriguez-Losada JA, Martinez-Frias J (2004) The felsic complex of the Vallehermoso Caldera: interior of an ancient volcanic system (La Gomera, Canary Islands). J Volcanol Geotherm Res 137:261–284

Rothe P (1968) Mesozoische Flysch-Ablagerungen auf Kanarieninsel Fuerteventura. Geol Rundsch 58:314–322

Sagan M (2018) A new approach to understanding the origin of Fuerteventura, Canary Islands (Spain): a U–Pb, Hf and O isotope and minor- and trace-element detrital zircon study. Master thesis, University of Alberta, p 141

Sagan M, Heaman LM, Pearson DG, Luo Y, Stern RA (2020) Removal of continental lithosphere beneath the Canary archipelago revealed from a U–Pb Age and Hf/O isotope study of modern sand detrital zircons. Lithos 362–363:1–18

Sagredo J, Muñoz M, Galindo C (1996) Caracteristicas petrológicas y edad K–Ar de las sienitas nefelinicas del Morro del Recogedero (Fuerteventura, Islas Canarias). Geogaceta 20:506–509

Santamarta JC, Expósito C, Eff-Darwich A (2014) Integration of green technologies in Canary Islands—low enthalpy geotermics. Local and regional challenges of climate change adaptation and green technologies, H-Sopron, 2014 ISBN 978-963-334-192-6

Schmincke H-U (1973) Magmatic evolution and tectonic regime in the Canaries, Madeira and Azores group. GSA Bull 84:633–648

Steiner C, Hobson A, Favre P, Stampfli GM, Hernandez J (1998) Early Jurassic sea-floor spreading in the Central Atlantic-the Jurassic Sequence of Fuerteventura (Canary Islands). GSA Bull 110:1304–1317

Steinthorsdottir M, Coxall H K, de Boer A M, Huber M, Barbolini N, Bradshaw CD et al (2021) The Miocene: The future of the past. Paleoceanogr Paleoclimatol 36:e2020PA004037. https://doi.org/10.1029/2020PA004037

Stillman CJ (1987) A Canary Islands Dyke Swarm: implications for the formation of oceanic islands by extensional fissural volcanism. In: Halls HC, Fahrig WF (eds) Mafic Dyke Swarms: Geol Assoc Canada Spec Paper, pp 34–54

Stillman CJ (1999) Giant Miocene landslides and the evolution of Fuerteventura, Canary Islands. J Volcanol Geotherm Res 94:89–104

Stillman CJ, Fúster JM, Bennell-Baker MJ, Muñoz M, Smewing JD, Sagredo J (1975) Basal Complex of Fuerteventura (Canary Islands) is an oceanic intrusive complex with rift-system affinities? Nature 257:469–471

Stockli DF, Farley KA, Dumitru TA (2000) Calibration of the apatite (U–Th)/He thermochronometer on an exhumed fault block, White Mountains, California. Geology 2:983–986

Uchupi E, Emery KO, Bowin CO, Phillips JD (1976) Continental margin of Western Africa: Senegal to Portugal. AAPG Bull 60:809–878

Urgeles R, Canals M, Baraza J, Alonso B, Masson DG (1997) The most recent megaslides on the Canary Islands: the El Golfo Debris Avalanche and the Canary Debris Flow, west El Hierro Island. J GeophyRes 102:20305–20323

Urgeles R, Canals M, Baraza J, Alonso B (1998) Seismostratigraphy of the western flanks of Hierro and La Palma (Canary Islands): a record of the Canary volcanism. Mar Geol 146:225–241

Urgeles R, Masson DG, Canals M, Watts AB, Le Bas T (1999) Recurrent large-scale landsliding on the west flank of La Palma, Canary Islands. J Geophys Res 104:25331–25348

Van den Bogaard P (2013) The origin of the Canary Island Seamount Province—new ages of old seamounts. Sci Rep 3:2107. https://doi.org/10.1038/srep02107

Watts AB, Masson DG (1995) A giant Landslide on the north flank of Tenerife, Canary Islands. J Volcanol Geotherm Res 100:24487–24498

Wipf M, Glasmacher UA, Stockli DF, Emmerich A, Bechstadt T, Baur H (2010) Reconstruction of the differentiated long-term exhumation history of Fuerteventura, Canary Islands, Spain, through fission track and (U–Th–Sm)/He data. Int J Earth Sci 99:675–686

Wolf RA, Farley KA, Silver LT (1996) Helium diffusion and low-temperature thermochronometry of apatite. Geochem Cosmochim Acta 60:4231–4240

Wolf RA, Farley KA, Kass DM (1998) Modelling of the temperature sensitivity of the apatite (U–Th)/He thermochronometer. Chem Geol 148:105–144

Zachos JC, Pagani M, Sloan L, Thomas E, Billups K (2001) Trends, rhythms, and aberrations in global climate 65 Ma to present. Science 292:686–693

Zachos JC, Dickens GR, Zeebe RE (2008) An early Cenozoic perspective on greenhouse warming and carbon-cycle dynamics. Nature 451:279–283. https://doi.org/10.1038/nature06588

Authors and Affiliations

Sherif Mansour[1,2] · Ulrich A. Glasmacher[1] · Florian C. Krob[1] · Ramón Casillas[3] · Marie Albinger[1]

[1] Institute of Earth Sciences, Heidelberg University, Heidelberg, Germany

[2] Geology Department, Faculty of Science, Port Said University, Port Said, Egypt

[3] Departamento de Biología Animal, Edafología y Geología, Universidad de La Laguna, La Laguna, Canary Islands, Spain